Production of bottomonia states in proton+proton and heavy ion collisions

Vineet Kumar[a], Prashant Shukla[a,b], Abhijit Bhattacharyya[c,*]

[a]*Nuclear Physics Division, Bhabha Atomic Research Centre, Mumbai 400085, India*
[b]*Homi Bhabha National Institute, Anushakti Nagar, Mumbai 400094, India*
[c]*Department of Physics, University of Calcutta, 92, A. P. C. Road Kolkata-700009, India*

Abstract

In this work, we review the experimental and theoretical developments of bottomonia production in proton+proton and heavy ion collisions. Bottomonia production process is proving to be one of the most robust processes to investigate the fundamental aspects of Quantum Chromodynamics at both low and high temperatures. The LHC experiments in last decade have produced large statistics of bottmonia states in wide kinematic range in various collision systems. The bottomonia have three Υ S-states which are reconstructed in dilepton invariant mass channel with high mass resolution by LHC detectors and P-states are measured via their decay to S-states. We start with the details of measurements in proton+proton collisions and their understanding in terms of various effective theoretical models. Here we cover both the Tevatron and LHC measurements with $\sqrt{s}$ spanning from 1.8 TeV to 13 TeV. The bottomonia states have particualrly been very good probes to understand strongly interacting matter produced in heavy ion collisions. The Pb+Pb collisions have been performed at various energies at LHC. This led to detailed study of the modification of bottominia yields as function of various observables and collision energy. At the same time, the improved results of bottomonia production became available from RHIC experiments which have proven to be useful for a quantitative comparison. A systematic study of bottomonia production in p+p, p+Pb and Pb+Pb have been very useful to understand the medium effects in these collision systems. We review some if not all the models of bottomonia evolution due to various processes in a large dynamically evolving medium and discuss these in comparison with the measurements.

Keywords: Beauty, Quarkonium, Bottomonium, Hadron Collision, Heavy-Ion Collision, Quark-Gluon Plasma, LHC, RHIC

*Corresponding author
Email address: abhattacharyyacu@gmail.com (Abhijit Bhattacharyya)

Contents

1. Introduction

The strong interaction among quarks and gluons is described by Quantum Chromodynamics (QCD) that has two regimes; asymptotic freedom at short distance and colour confinement at long distances. At short distance, the interaction can be well described using perturbative methods. However, confinement, which is a non-perturbative phenomenon, is not very well understood. The study of quarkonia ($Q\bar{Q}$) involves both the perturbative and non-perturbative aspects of QCD. The quarkonia are composed of heavy constituents (charm and bottom quarks) and their velocity can be considered small allowing to use non-relativistic formalism [1, 2] in the study. In a simple picture, a quarkonium can be understood as a heavy quark pair ($Q\bar{Q}$) bound in a colour singlet state by some effective potential interaction. In this bound state, the constituents are separated by distances much smaller than $1/\Lambda_{\rm QCD}$ where $\Lambda_{\rm QCD}$ is the QCD scale.

It is expected that the dynamics of strongly interacting matter changes at temperatures and/or densities which are similar to or larger than the typical hadronic scale. It can be argued that under such extreme conditions, one should have the onset of deconfinement of quarks and gluons and thus the strongly-interacting matter could then be described in terms of these elementary degrees of freedom. This new form of matter is known as quark-gluon plasma [3, 4], or QGP. The support for the existence of such a transition has indeed been demonstrated from first principles using QCD simulation on lattice. The heavy ion collisions provide experimental means to study the deconfinement transition and the properties of hot and dense strongly-interacting matter [5] Significant parts of different experimental heavy-ion programmes are dedicated to studying quarkonium yields. Such studies are motivated by the suggestion of Matsui and Satz that quarkonium suppression could be a signature of deconfinement [6]. In fact, the observation of anomalous suppression of J/ψ at SPS energies was considered to be a key signature of deconfinement [7].

The Υ's having three states with different binding energies are far richer probes of the QCD dynamics in p+p and Pb+Pb collisions than the charmonia states. It is therefore important to achieve a good understanding of their production mechanism in the vacuum as well as of how the nuclear effects in proton-nucleus collisions affect them. At Large Hadron Collider (LHC) energy, the cross section of bottomonia production is large and also the detector technologies enabled the study of various bottomonia states separately both in p+p and heavy ion collisions. As proposed by different theories, bottomonium is an important and clean probe of hadronic collisions for at least two reasons. First, the effective field theory approach, which provides a link to first principles QCD, is more suitable for bottomonium due to better separation of scales and higher binding energies. Second, the statistical recombination effects are less important due to the higher mass of bottom quarks. Experimentally, the bottomonia are detected via their decay in dimuon channel which which can be reconstructed with better mass resolution and smaller combinatorial background due to higher mass as compared to other resonances. All these properties make bottomonium a good probe of QGP formation in heavy ion collisions.

The detailed experimental study of the bottomonia states in p$\overline{\rm p}$ collisions were carried at Fermilab at $\sqrt{s}$ = 1.8 and 1.96 TeV [8, 9, 10]. LHC carried out the bottomonia study in p+p collisions at $\sqrt{s}$ = 7 TeV [11, 12, 13] and 13 TeV [14, 15]. There have been immense experimental [16, 17, 18, 19, 20] and theoretical works [21, 22, 23, 24] on quarkonia modifications in Pb+Pb collisions. The botomonia states in heavy ion collisions are suppressed with respect to their yields in proton-proton collisions scaled by the number of binary nucleon-nucleon (NN) collisions. The amount of quarkonia suppression is expected to be sequentially ordered by the binding energies of the quarkonia states. As the screening depends on the binding energy the bottomonium states (Υ(1S), Υ(2S), Υ(3S), χ_b, etc.) are extremely useful probes to understand the color screening properties of the QGP. The sequential suppression of the yields of Υ(nS) states was first observed by CMS at $\sqrt{s_{_{NN}}}$ =2.76 TeV [25, 26]. Later, the results with improved statistical precision have been reported by both the ALICE [20] and CMS Collaborations [17, 18] at $\sqrt{s_{_{NN}}}$ =5.02 TeV. The suppression of the Υ(1S) meson has also been studied at $\sqrt{s_{_{NN}}}$ =200 GeV at Relativistic Heavy Ion Collider (RHIC) [27], although the bottomonia production cross section is small at lower energies.

In this writeup, we review experimental and theoretical aspects of bottomonia production in p+p, p+A and A+A collisions at RHIC and LHC energies.

2. Bottomonia production in p+p collisions: Experimental overview

In this section, we will give an overview of measurements of Υ production in p+p collisions at LHC and p$\overline{\rm p}$ collisions at Tevatron.

The Υ meson was discovered by E288 collaboration at Fermilab in the collision of a beam of 400 GeV protons with nucleus in 1977 [28]. The detailed measurements of all the states of Υ were also done at Fermilab. The Collider Detector at Fermilab (CDF) measured Υ(1S), Υ(2S) and Υ(3S) differential ($d^2\sigma/dp_T dy$) and integrated cross sections in p$\overline{\rm p}$ collisions at $\sqrt{s}$ = 1.8 TeV [8] at Tevatron. The three states were reconstructed via their decays to μ^+ and μ^-. The differential ($d^2\sigma/dp_T dy$) and integrated cross sections have been measured for Υ(1S) in the transverse momentum range 0<p_T<16 GeV/c and for Υ(2S) and Υ(3S) in the range 0<p_T<10 GeV/c. In 2002, CDF measured both the cross sections and polarizations of Υ for $|y|$< 0.4 in p$\overline{\rm p}$ collisions at $\sqrt{s}$ = 1.8 TeV with an integrated luminosity of 77 pb^{-1} [9]

Table 1: The cross section of Υ(nS) at midrapidity ($|y|< 0.4$) in p$\overline{\text{p}}$ collisions at $\sqrt{s}$ = 1.8 TeV with an integrated luminosity of 77 pb^{-1} as measured by CDF [9]

Υ(nS) state	$\frac{d\sigma(\Upsilon(nS))}{dy} \times B(\Upsilon(nS) \to \mu^+\mu^-)$ (pb)
Υ(1S)	680±15(stat.)±18(syst.)±26(lumi.)
Υ(2S)	175±9(stat.)±8(syst.)
Υ(3S)	97±8(stat.)±5(syst.)

Table 2: Υ(1S) cross sections in different rapidity ranges in p$\overline{\text{p}}$ collisions at $\sqrt{s}$ = 1.96 TeV measured in Tevatron Run II at luminosity of 185 pb^{-1} [10].

rapidity range	$\frac{d\sigma(\Upsilon(1S))}{dy} \times B(\Upsilon(nS) \to \mu^+\mu^-)$ (pb)
0.0-0.6	628±16(stat.)±63(syst.)±38(lumi.)
0.6-1.2	654±17(stat.)±65(syst.)±40(lumi.)
1.2-1.8	515±16(stat.)±46(syst.)±31(lumi.)
0.0-1.8	597±12(stat.)±58(syst.)±36(lumi.)

and the cross sections are listed in Table 1. These studies helped to understand the relative production of Υ states in hadronic collisions.

The Run II of Tevatron was carried out at p$\overline{\text{p}}$ collisions at $\sqrt{s}$ = 1.96 TeV, and D0 experiment published results from these experiments. D0 experiment measured Υ(1S) cross section in different rapidity ranges in p$\overline{\text{p}}$ collisions at $\sqrt{s}$ = 1.96 TeV at luminosity of 185 pb^{-1} [10]. Table 2 summarizes the D0 Υ cross section measurements.

The measurements of the production of Υ(1S,2S,3S) in p+p collisions at the unprecedented center of mass energies of 2.76, 5.02, 7, 8, and 13 TeV have been undertaken, within various rapidity windows and in the dimuon momentum range of $p_T < 100$ GeV/c at LHC by ATLAS [29, 13], CMS [30, 14] and LHCb collaborations [15].

The Large Hadron Collider (LHC) performed Upsilon measurements at $\sqrt{s}$ = 7 TeV in p+p collisions that is rougly four times of the Tevatron energy. CMS measured the Υ cross section in 2011 in kinematic range $|y|< 2$, and $p_T< 30$ GeV [11] with a luminosity of 3.1 pb^{-1}. In 2013, CMS measured the Υ cross section in p+p collisions at $\sqrt{s}$ =7 TeV with increased luminosity of 35.8 pb^{-1} and in the kinematic range $|y|< 2.4$ and $p_T< 50$ GeV [12] as shown in Table 3.

Table 3: Υ(nS) cross sections in kinematic range $|y|< 2.0$ and $p_T< 50$ GeV measured by CMS in p+p collisions at $\sqrt{s}$ =7 TeV. for luminosity of 35.8 pb^{-1} [12].

Υ(nS) state	$\sigma(p+p \to \Upsilon(nS)X) \times B(\Upsilon(nS) \to \mu^+\mu^-)$ (nb)
Υ(1S)	8.55±0.05(stat.)$^{+0.56}_{-0.50}$(syst.)±0.34(lumi.)
Υ(2S)	2.21±0.03(stat.)$^{+0.16}_{-0.14}$(syst.)±0.09(lumi.)
Υ(3S)	1.11±0.02(stat.)$^{+0.10}_{-0.08}$(syst.)±0.04(lumi.)

Table 4: ATLAS measurement of Υ(nS) cross section in $|y|<$ 2.25 and $p_T<$ 70 GeV at $\sqrt{s}$ =7 TeV [13].

Υ(nS) state	$\sigma(p+p \to \Upsilon(nS)X) \times B(\Upsilon(nS) \to \mu^+\mu^-)$ (nb)
Υ(1S)	8.01$\pm$0.02(stat.)$\pm$0.36(syst.)$\pm$0.31(lumi.)
Υ(2S)	2.05$\pm$0.01(stat.)$\pm$0.12(syst.)$\pm$0.08(lumi.)
Υ(3S)	0.92$\pm$0.01(stat.)$\pm$0.07(syst.)$\pm$0.04(lumi.)

The ATLAS experiment measured the Υ(nS) production cross section in p+p collisions at $\sqrt{s}$ =7 TeV in kinematic range $|y|<$ 2.25, and $p_T<$ 70 GeV [13]. The results are shown in table 4.

Several Υ polarization measurements have also been made. With a luminosity of 77 pb^{-1}, CDF measured the Υ(1S) polarization in 2002 in p$\overline{\text{p}}$ collisions at $\sqrt{s}$ =1.8 TeV in knematic range $|y|<$ 0.4 and found that Υ(1S) is unpolarized [9]. At $\sqrt{s}$ = 1.96 TeV, D0 experiment measured the Υ(1S) and Υ(2S) polarizations in 2008 in p$\overline{\text{p}}$ data with a luminosity of 1.3 fb^{-1} [31]. The measurement done by D0 found longitudinal polarization for the Υ(1S) [31]. However, these first polarizations measurements were only done in one reference frame. They were sensitive to the bias resulted due to the choice of the reference frame and also to the acceptance of the detector. Later, measurements were done in multiple reference frames which enabled the calculation of the frame invariant parameter to prevent bias from the choice of reference frame and detector acceptance.

The first full polarizations for all Υ(nS) states were measured in 2012 by CDF in Tevatron Run II at $\sqrt{s}$ = 1.96 TeV [32]. The CDF Run II measurement with a luminosity of 6.7 fb^{-1} with $|y|<$ 0.6 and $p_T<$ 40 GeV found no evidence for polarization [32]. CMS measured the Υ(nS) polarization in 2003 in p+p collisions at $\sqrt{s}$ = 7 TeV with a luminosity 4.9 fb^{-1} [33]. In these measurements, the angular distribution of the muons produced in the Υ(1S, 2S, 3S) decays were analyzed in different reference frames to determine the polarization parameters. The CMS polarization measurements found the Υ to be unpolarized and suggested that this could be a result of including Υ produced in feeddown from an excited state [33].

CMS measured the differential cross-section of Υ(nS) in p+p collisions at $\sqrt{s}$ = 13 TeV in central rapidities $|y| < 2.4$, as a function of transverse momentum in high momentum range [14]. These are used to constrain the theoretical calculations in the high momentum range as shown in the next section 3.

The Υ(nS) cross sections are measured by LHCb [15] in p+p collisions at $\sqrt{s} = 13$ TeV, in transverse momentum range $0 < pT < 15$ GeV/c and forward rapidity region $2 < y < 4.5$. The cross sections are listed here.

B(Υ(1S) $\to \mu^+\mu^-$) $\times$ σ(Υ(1S)) = 4687 $\pm$ 10 $\pm$ 294 pb,

B(Υ(2S) $\to \mu^+\mu^-$) $\times$ σ(Υ(2S)) = 1134 $\pm$ 6 $\pm$ 71 pb, B(Υ(3S) $\to \mu^+\mu^-$) $\times$ σ(Υ(3S)) = 561 $\pm$ 4 $\pm$ 36 pb.

The measurements of the cross sections and polarizations have shed light on the Υ(1S, 2S, 3S) production mechanisms in p+p collisions. LHC data has substantially extended the reach of the kinematics to test the Non-Relativistic QCD (NRQCD) and other models with higher-order corrections which becomes more distinguishable with the increase of p_T,

3. Bottomonia production mechanism in p+p collisions

In general, one can subdivide the quarkonia production process into two major parts; production of a heavy quark pair in hard collisions and formation of quarkonia out of the two heavy quarks. The massive quarks (with $m_c \sim 1.6$ GeV/c^2, $m_b \sim 4.5$ GeV/c^2) are produced in initial stages in hadronic collision with high momentum transfer and can be treated perturbatively [34]. The formation of quarkonia from the two massive quarks, is a non-perturbative phenomenon which is described using different effective models [35, 36]. The Colour Singlet Model (CSM) [37, 38], Colour Evaporation Model (CEM) [39, 40], the Fragmentation Scheme and the NRQCD factorisation formalism are some of the popular approaches used for quarkonia production.

The hadronic cross section in $p+p$ collisions at center of mass energy $\sqrt{s}$ can be written as

$$\sigma_{pp}(s, m^2) = \sum_{i,j=q,\overline{q},g} \int dx_1\, dx_2\, f_i^p(x_1, \mu_F^2)\, f_j^p(x_2, \mu_F^2)\, \widehat{\sigma}_{ij}(\hat{s}, m^2, \mu_F^2, \mu_R^2) \tag{1}$$

Here, f_i^p are the parton ($i = q, \overline{q}, g$) densities of the proton, x_1 and x_2 are the fractional momenta carried by the colliding partons and μ_F and μ_R are, respectively, fragmentation and renormalization scales. The total partonic cross section has been calculated up to NLO [34, 41] and can be expressed as

$$\begin{aligned}\widehat{\sigma}_{ij}(\hat{s}, m, \mu_F^2, \mu_R^2) &= \frac{\alpha_s^2(\mu_R^2)}{m^2}\Big\{ f_{ij}^{(0,0)}(\rho) \\ &+ 4\pi\alpha_s(\mu_R^2)\left[f_{ij}^{(1,0)}(\rho) + f_{ij}^{(1,1)}(\rho)\ln\left(\frac{\mu_F^2}{m^2}\right)\right] + \mathcal{O}(\alpha_s^2)\Big\}\end{aligned} \tag{2}$$

where $\rho = 4m^2/\hat{s}$ and $f_{ij}^{(k,l)}$ are the scaling functions to NLO [34, 41]. At small ρ, the $\mathcal{O}(\alpha_s^2)$ and $\mathcal{O}(\alpha_s^3)$ $q\overline{q}$ and the $\mathcal{O}(\alpha_s^2)$ gg scaling functions become small while the $\mathcal{O}(\alpha_s^3)$ gg and qg scaling functions plateau at finite values. Thus, at collider energies, the total cross sections are primarily dependent on the small x parton densities and phase space. The total cross section does not depend on any kinematic variables. It depends only on the quark mass, m, and the renormalization and factorization scales with central values $\mu_{R,F} = \mu_0 = m$.

The formation of quarkonium through a nonperturbative evolution of the $Q\bar{Q}$ pair has been discussed extensively using different models and also in the framework of the effective field theories of QCD [35, 42]. Different treatments of this evolution have led to various theoretical models for inclusive quarkonium production. Most notable among these are the color-singlet model (CSM), the color-evaporation model (CEM) and the non-relativistic QCD (NRQCD) factorization approach. In this review, we will describe CEM and NRQCD approaches and their results in comparison with the measurements

3.1. The color singlet model

The color singlet model (CSM) was proposed shortly after the discovery of the J/ψ [37, 38, 43, 44]. In CSM model, it is assumed that the $Q\bar{Q}$ pair which evolves into the quarkonium is in a color-singlet state and also the pair has the same spin and angular-momentum quantum numbers as the final quarkonium. In the CSM, the production rate for quarkonium state is obtained in terms of of the absolute values of the color-singlet $Q\bar{Q}$ wave function and its derivatives, evaluated at zero $Q\bar{Q}$ separation. These quantities can be extracted by comparing theoretical calculations in the CSM with experimental measurements. Once these quantities are extracted the CSM can predict the cross sections at any given collision energy. At low energies, the CSM can successfully predict the quarkonium production cross sections [45]. But, at high energies, very large corrections to the CSM appear at next-to-leading order (NLO) and next-to-next-to-leading order (NNLO) in α_s [46, 47, 48]. It thus indicate that there may be some additional production mechanism emerging at high energy. However, given the very large corrections at NLO and NNLO, it is not clear that the perturbative expansion in α_s is convergent.

3.2. The color evaporation model

The CEM [39, 40, 49] is motivated by the principle of quark-hadron duality. In the CEM, it is assumed that every produced $Q\overline{Q}$ pair can evolve into a quarkonium if it has an invariant mass that is less than the threshold for producing a pair of open-flavor heavy mesons. It is further assumed that the nonperturbative probability for the $Q\overline{Q}$ pair to evolve into a quarkonium state H is given by a constant F_H that is independent of energy-momentum and process. Once F_H has been fixed by comparison with the measured total cross section for the production of the quarkonium H, the CEM has no more free parameters and can predict, the momentum distribution of the quarkonium production rate at any collision energy. The CEM predictions provide good descriptions of the CDF data for J/ψ, $\psi(2S)$ and χ_c production at $\sqrt{s} = 1.8$ TeV [49].

Table 5: Heavy quark and quarkonia production cross sections at $\sqrt{s_{NN}}$ = 5.02 TeV. The cross sections are given per nucleon pair while $N^{\rm PbPb}$ gives the initial number of heavy quark pair/quarkonia per Pb+Pb event.

	$b\bar{b}$	Υ
σ_{pp}	$210.3^{+70.8}_{-77.6}$ μb	$0.42^{+0.14}_{-0.16}$ μb
$\sigma_{\rm PbPb}$	$179.3^{+60.3}_{-66.2}$ μb	$0.359^{+0.121}_{-0.132}$ μb
$N^{\rm PbPb}$	$1.007^{+0.339}_{-0.372}$	$0.0020^{+0.0007}_{-0.0007}$

The quarkonium production cross sections are calculated in the color evaporation model with normalizations determined from fitting the scale parameter to the shape of the energy-dependent cross sections in Ref. [50]. The production cross sections for heavy flavor and quarkonia at $\sqrt{s_{\rm NN}}$ = 5.02 TeV [51] calculated using CEM are given in Table 5. The heavy quark production cross section are calculated to NLO in pQCD using the CT10 parton densities [52]. The botttom quark mass and scale parameters are $m_b = 4.65 \pm 0.09$ GeV, $\mu_F/m_{T\,b} = 1.40^{+0.75}_{-0.47}$, and $\mu_R/m_{T\,b} = 1.10^{+0.26}_{-0.19}$. The central EPS09 NLO parameter set [53] is used to calculate the modifications of the parton distribution functions (nPDF) in Pb+Pb collisions, referred as cold nuclear matter (CNM) effects. The yields in a minimum bias Pb+Pb event is obtained from the per nucleon cross section, $\sigma_{\rm PbPb}$, in Table 5, as

$$N = \frac{A^2 \sigma_{\rm PbPb}}{\sigma^{\rm tot}_{\rm PbPb}} \; . \quad (3)$$

At 2.76 TeV, the total Pb+Pb cross section, $\sigma^{\rm tot}_{\rm PbPb}$, is 7.65 b [54].

Recently, work in Ref. [55] presents Improved Color Evaporation Model (ICEM). They obtained bottomonium production cross sections as a function of transverse momentum and rapidity and calculate the polarization of prompt $\Upsilon(n{\rm S})$ production at leading order employing the k_T-factorization approach. We reproduce here some of the representative calculations using ICEM.

Figure 1 shows the differential cross section for Υ(1S) production as a function of p_T in p+p collisions at $\sqrt{s}$ = 7 TeV in midrapidity, $|y| < 2.4$, calcuated using ICEM [55] with combined mass and renormalization scale uncertainties (blue). Also shown are the calculations with CEM using collinear factorization approach (magenta). The calculations are compared with the CMS midrapidity data [30].

Figure 2 shows the differential production cross sections of prompt Υ(2S) (left) and prompt Υ(3S) (right) as a function of p_T in p+p collisions at $\sqrt{s}$ = 7 TeV in midrapidity, $|y| < 2.4$, calculated using ICEM [55] with combined mass and renormalization scale uncertainties compared with the CMS midrapidity data [30].

These results show that the p_T dependence of the cross sections of all three states are explained by ICEM within the model uncertainties. The model gives probability F_H for the $Q\overline{Q}$ pair to evolve into a

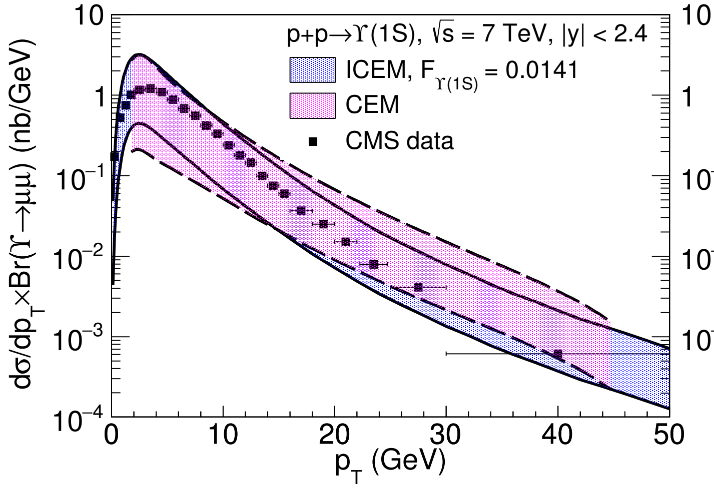

Figure 1: (Color online) The differential cross section for Υ(1S) production as a function of p_T in p+p collisions at $\sqrt{s}$ = 7 TeV in midrapidity $|y| < 2.4$ calcuated using ICEM [55] with combined mass and renormalization scale uncertainties (blue). Also shown the are calculations with CEM using collinear factorization approach (magenta). The calculations are compared with the CMS midrapidity data [30].

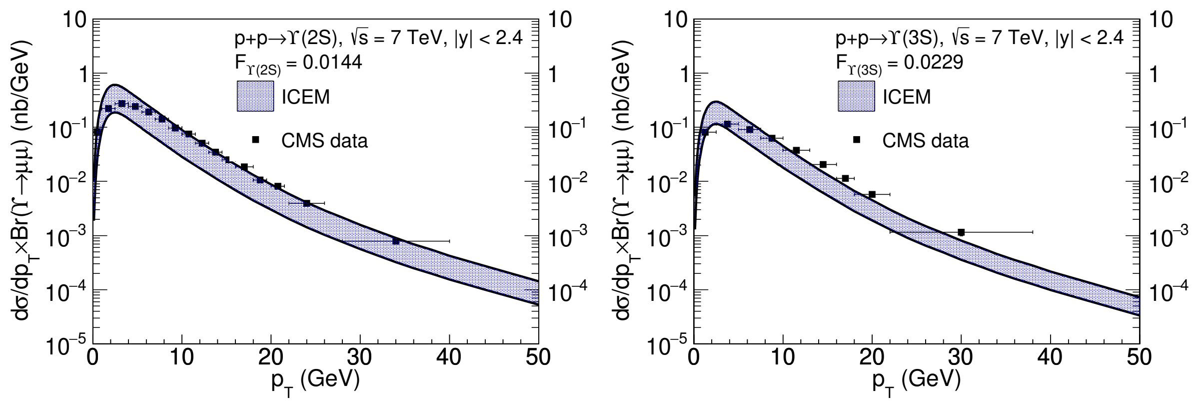

Figure 2: (Color online) The differential production cross sections of prompt Υ(2S) (left) and prompt Υ(3S) (right) as a function of p_T in p+p collisions at $\sqrt{s}$ = 7 TeV in midrapidity, $|y| < 2.4$ calculated using ICEM [55] with combined mass and renormalization scale uncertainties compared with the CMS midrapidity data [30].

quarkonium state H.

3.3. The NRQCD factorization approach

The $Q\bar{Q}$ pair, evolving into the quarkonium, is assumed to have same spin and angular momentum same as that of quarkonium. NRQCD approach incorporates both the colour singlet as well as the Colour Octet (CO) states of quarkonium. In the formalism of the NRQCD factorisation approach, the evolution probability of $Q\bar{Q}$ pair into a state of quarkonium is expressed as matrix elements of NRQCD operators. These operators are expanded in terms of the velocity v (for $v \ll$1) of heavy quarks [35]. The production cross-sections and decay rates of quarkonia states are then calculated using factorisation formulae. The full structure of the $Q\bar{Q}$ Fock space is spanned by n=${}^{2s+1}L_J^{[a]}$ state where L is the orbital angular momentum, s is the spin, J is the total angular momentum and a (colour multiplicity) = 1 for CS and 8 for CO states.

The produced CO states of $Q\bar{Q}$ pair at short distances finally emerge as CS quarkonia by emitting soft gluons non-perturbatively.

There have been several studies on bottomonia production based on NRQCD formalism [56, 57, 58, 59, 60]. Both the production and polarisation of Υ(nS) at NLO have been discussed in Ref. [61] within the framework of NRQCD. The CO matrix elements are obtained by fitting the calculations with experimental data. The study is updated in Ref. [62] by considering feed down from χ_{bJ}(mP) states in Υ(nS) production. The yields and polarisations of Υ(nS) measured at Tevatron and LHC are well explained by this work. The NLO study in Ref. [63] includes feed down contributions from higher states and describes the cross sections and polarisations of Υ(nS) at LHC energy. In Ref. [64], production cross-section for Υ(nS), χ_{bJ}, η_b and h_b have been calculated using NRQCD, as produced in hard photo production and fragmentation processes at LHC energies. In Ref. [65] it is shown that there is a large difference among the Long Distance Matrix Element (LDME)s obtained by different analysis at NLO.

In Ref. [65] the LO NRQCD calculations for the differential production cross-sections of Υ states in p+p collisions have been discussed. This work uses a large set of data from Tevatron [66] and LHC [30, 67, 12, 13, 14] to extract the LDMEs required for the Υ production. It is to be noted that an LO NRQCD analyis is straightforward and has excellent predictability power for unknown cross sections.

The processes that govern the production of heavy mesons like bottomonium, can be denoted generically by $i + j \to \Upsilon + X$, where i and j are the incident light partons, Υ is the heavy meson and X is final state light parton. The double differential cross-section as a function of p_T and rapidity (y) of the heavy meson can be written as [68],

$$E\frac{d^3\sigma^{\Upsilon}}{d^3p} = \sum_{i,j=q,\bar{q},g}\int dx_1 dx_2 f_i^p(x_1,\mu_F^2) f_i^p(x_2,\mu_F^2)\delta(s+u+t-m^2)\frac{\hat{s}}{\pi}\frac{d\sigma}{d\hat{t}} \tag{4}$$

where, $f_i^p(f_j^p)$ are distribution functions of the colliding parton $i(j)$ in the incident protons as a function of $x_1(x_2)$; the fractions of the total momentum carried by the incident partons and the scale of factorisation μ_F. Here $\sqrt{s}$ is the total center of mass energy of the p+p system and m_T $(= \mu_F)$ stands for the transverse mass, $m_T^2 = p_T^2 + M^2$ of the quarkonium. The $d\sigma/d\hat{t}$ in Eq. 4 is the parton level cross-section and is defined as [35],

$$\frac{d\sigma}{d\hat{t}} = \frac{d\sigma}{d\hat{t}}(ab \to Q\bar{Q}(^{2s+1}L_J) + X) M_L(Q\bar{Q}(^{2s+1}L_J) \to \Upsilon) \tag{5}$$

The first term in RHS is the short distance contribution, that corresponds to the $Q\bar{Q}$ pair production in specific colour and spin configuration and is calculable using perturbative QCD (pQCD) [58, 69, 70, 71, 72,

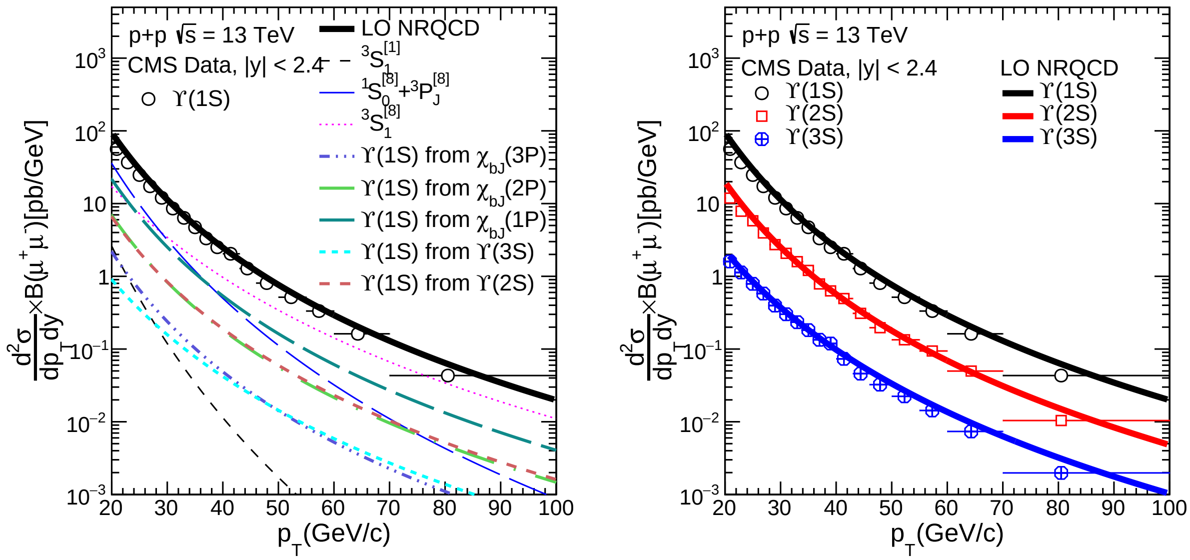

Figure 3: (Color online) The NRQCD calculations [65] of production cross-section of Υ(nS) in p+p collisions at $\sqrt{s}$ = 13 TeV in central rapidities, as a function of transverse momentum compared with the measured data at CMS [14] experiment. The left figure shows relative contributions in Υ(1S) from singlet and octet states as well as from feeddown. The right figure shows the sum of all contributions for all the 3 states where the results for Υ(1S) and Υ(2S) are shifted vertically by a constant factors, for better visibility.

73]. The other term in the RHS of Eq.(5) is the LDME and gives the probability of the $Q\bar{Q}$ state to convert into a quarkonium state. They are determined by comparing the calculations with the measurements.

The quarkonium yield depends on the ${}^3S_1^{[1]}$ and ${}^3P_J^{[1]}$(J=0,1,2) CS states and ${}^1S_0^{[8]}$, ${}^3S_1^{[8]}$ and ${}^3P_J^{[8]}$ CO states in the limit $v \ll 1$. The superscripts in square brackets represent the colour structure of the bound state, 1 for the CS and 8 for the CO.

One requires both CS and CO matrix elements in order to get theoretical predictions for the production of bottomonia at the Tevatron and LHC energies. The corresponding expressions and numerical values for CS states are obtained from Ref. [58]. The CO states are obtained using experimentally measured data sets as in Refs. [58, 72, 73]. For the CO elements related to p-wave states, needed as the feed down contributions, are obtained by Ref. [60, 62].

Here we present the NRQCD results obtained in Ref. [65]. The calculations use CT18NLO parametrisation [74] for parton distribution functions and the bottom quark mass m_b is taken to be 4.88 GeV. Measured transverse momentum distributions of Υ(3S), Υ(2S) and Υ(1S) in p +p̄ collisions at $\sqrt{s} = 1.8$ TeV and in p+p collisions at 7 TeV and 13 TeV are used to constrain the LDMEs.

Figure 3 shows the NRQCD calculations of production cross-section of Υ(nS) in p+p collisions at $\sqrt{s}$ = 13 TeV in central rapidities, as a function of transverse momentum compared with the measured data at CMS [14] experiment. The left figure shows relative contributions in Υ(1S) from singlet and octet states

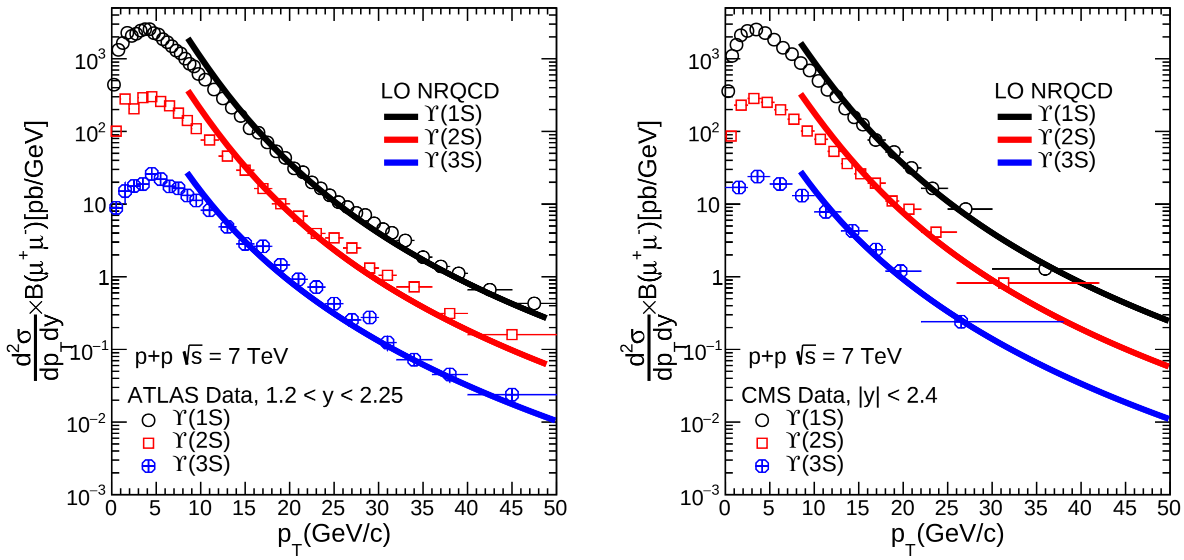

Figure 4: (Color online) The NRQCD calculations [65] of production cross-section of Υ(nS) in p+p collisions at $\sqrt{s}$ = 7 TeV, as a function of transverse momentum compared with the measured data by ATLAS [13] in left figure and CMS [30] in right figure. The cross-section of Υ(1S) and Υ(2S) as well as calculations are shifted vertically by a constant factors for better visibility.

Table 6: Comparison of CS elements and CO LDMEs extracted from fitting with experimental data using NRQCD formalism for Υ(1S).

Ref. (LO/NLO)	PDF	m_b (GeV)	$M_L(bb([^3S_1]_1 \rightarrow \Upsilon(1S)$ (GeV^3)	$M_L(bb([^3S_1]_8 \rightarrow \Upsilon(1S)$ (GeV^3)	$M_L(bb([^1S_0]_8,$ $[^3P_0]_8 \rightarrow \Upsilon(1S)$ (GeV^3)	p_T-cut GeV/c
[65] (LO)	CT18	4.88	10.9	0.0601±0.0017	0.0647±0.0016	8
[57] (LO)	CTEQ4L	4.88	11.1	0.077±0.017	0	2
				0.087±0.016	0	4
				0.106±0.013	0	8
[58] (LO)	CTEQ5L	4.77	12.8±1.6	0.116±0.027	0.109±0.062	8
				0.124±0.025	0.111±0.065	
	MRSTLO	4.77	12.8±1.6	0.117±0.030	0.181±0.072	8
				0.130±0.028	0.186±0.075	
[60] (LO)	MSTW08LO	4.88	10.9	0.0477±0.0334	0.0121±0.0400	-
[61] (NLO)	CTEQ6M	4.75	9.282	-0.0041±0.0024	0.0780±0.0043	8
[62] (NLO)	CTEQ6M	PDG	9.282	0.0061±0.0024	0.0895±0.0248	8

as well as from feeddown. The right figure shows the sum of all contributions for all the 3 states where the results for Υ(1S) and Υ(2S) are shifted vertically by a constant factors for better visibility.

Figure 4 shows the NRQCD calculations of production cross-section of Υ(nS) in p+p collisions at $\sqrt{s}$ = 7 TeV, as a function of transverse momentum compared with the measured data by ATLAS [13] in left figure and CMS [30] in right figure. The cross-section of Υ(1S) and Υ(2S) as well as calculations are shifted vertically by a constant factors for better visibility.

The calculations for Υ(3S), Υ(2S) and Υ(1S) are compared with the measured data at Tevatron and LHC. The NRQCD formalism provides very good description of the data in large transverse momentum range at different collision energy. At high p_T, the colour singlet contribution is very small and LHC data in large p_T range help to constrain the relative contributions of different colour octet contributions.

Table 6 summarizes the LDME values for Υ(1S) obtained by different groups.

3.4. Additional methods

In this section we, very briefly, touch upon two specialized processes namely i) Fragmentation and ii) k_T factorisation.

Fragmentation. In heavy ion collisions at high energies, the produced partons carry large transverse momentum. When such a parton with large transverse momentum (k_T) decays into the final hadronic state (quarkonium state here) [75] then the process of production is called fragmentation. At large enough k_T, quarkonium production is dominated by fragmentation instead of the short distance mechanism which is suppressed by powers of m_Q/k_T even though fragmentation is of higher order in α_s [75]. It was first shown by Braaten and Yuan [75, 76] that fragmentation of gluons and heavy quarks could be an important source of large-k_T quarkonia production. A process like $AB \to HX$ (where A, B are hadrons) is factorised into a part containing the hard-scattering cross-section which produces a gluon or a heavy quark and a part which takes care of the fragmentation of the gluon or the heavy quark into the relevant quarkonia state. One may write

$$d\sigma(AB \to HX) = \sum_i \int_0^1 dz\; d\sigma(AB \to iX)\; D_{i\to H}(x,\mu). \tag{6}$$

In the above equation, i is either a gluon or a heavy quark. The term $D_{i\to H}(x,\mu)$ is called the fragmentation function which depends on the fraction (x) of momentum of the parent parton carried by the quarkonia state and the scale μ which is of the order of k_T.

k_T factorisation. Another approach to quarkonium production is the k_T factorisation method [77, 78]. In the standard collinear approach, it is assumed that the momentum of all partons is in the same direction as the initial particle and thus the transverse momentum (k_T) is considered to be zero. But, at large collision energies, the transverse momentum (k_T) is not negligible at all.

In the k_T factorisation approach, the quarkonium cross section is factorised into two parts, a cross section $\hat{\sigma}(x, k_T, \mu)$ and a parton density function $f(x, k_T, \mu)$, where both depend on the transverse momentum k_T [79]. The quarkonium cross section is given by

$$\begin{aligned} \sigma &= \sum_{i,j} \int \frac{dx_1}{x_1} \frac{dx_2}{x_2}\, f_i(x_1, k_{T,1}^2, \mu)\, f_j(x_2, k_{T,2}^2, \mu) \\ &\quad \times \hat{\sigma}_{i+j\to H}(k_{T,1}, k_{T,2}, x_1, x_2, s)\, dk_{T,1}^2\, dk_{T,2}^2 \end{aligned} \tag{7}$$

where i and j are initial partons, H is the final state, and $\hat{\sigma}_{i+j\to H}$ is the parton cross section giving the probability that initial partons i and j will form final state H.

4. Experimental overview of Bottomonia results in heavy ion collisions

4.1. Υ(nS) Nuclear Modification Factor R_{AA}

A large set of heavy ion collisions data is available at both RHIC and LHC energies. RHIC at BNL is designed for Au+Au collisions at $\sqrt{s_{\rm NN}}$ = 200 GeV and can accelerate ions upto Uranium. Both PHENIX and STAR experiments at RHIC can measure quarkonia in dimuon channel. LHC runs part of the time for heavy ion program and it can perform Pb+Pb collision upto $\sqrt{s_{\rm NN}}$ = 5.5 TeV. In addition, d+Au collisions are performed at RHIC and p+Pb collisions are performed at LHC to study intermediate system. The CMS, ATLAS and ALICE detectors at LHC have obtained large amount of Upsilon data in different kinematic ranges.

To quantify the effect of medium in the quarkonia production scenario, one takes recourse to a quantity called the nuclear modification factor (R_{AA}). This quantity is defined as the ratio of the quarkonium yield in the A+A collisions to that in p+p collisions scaled by the average number of collisions $\langle N_{\rm coll}\rangle$:

$$R_{AA} = \frac{1}{\langle N_{\rm coll}\rangle} \frac{N_{AA}^{Q\bar{Q}}}{N_{pp}^{Q\bar{Q}}}. \tag{8}$$

The ratio will be unity if the physics of the A+A collisions is simply the sum of a scaled number of p+p collisions. The effect of the medium should make it vary from unity. In this section, we review the current status of the experimental measurement of nuclear modification factor of the Υ states. The results

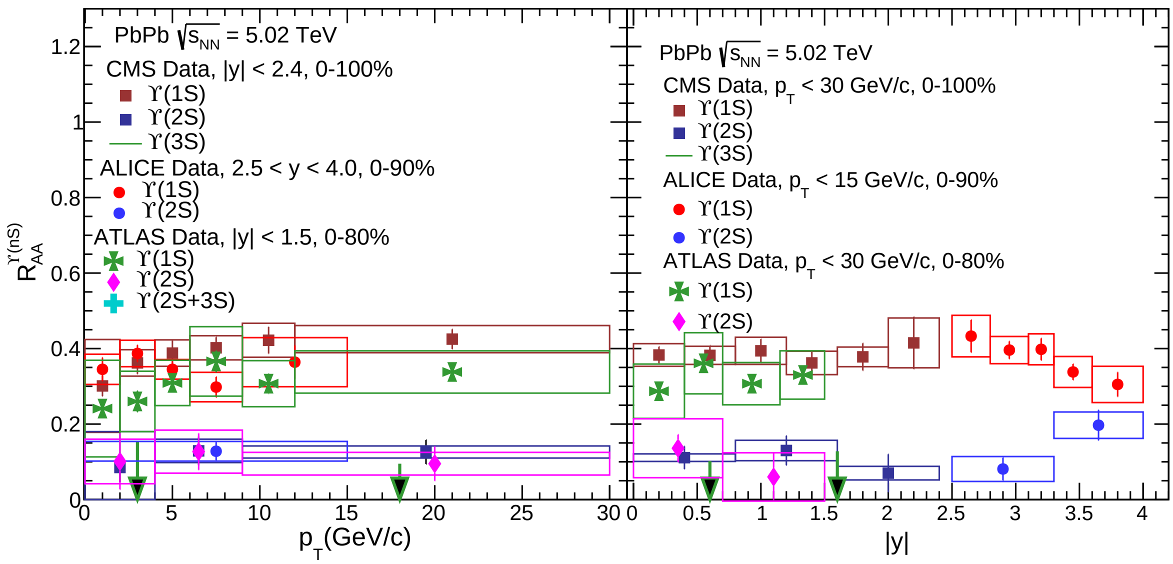

Figure 5: (Color online) The Υ(nS) nuclear modification factor, R_{AA} in Pb+Pb collisions at $\sqrt{s_{\rm NN}}$ = 5.02 TeV, (a) as a function of transverse momentum p_T and (b) as a function of rapidity measured by CMS [18], ALICE [82] and ATLAS experiments [82]. The vertical bars denote statistical uncertainties, and the rectangular boxes show the total systematic uncertainties.

from different experiments are compared to understand effects of the medium and their dependence on the collision energy and kinematic ranges.

The cross sections of bottomonia at LHC are large and hence all the bottomonia states (Υ(nS)) are measured at the LHC with very good statistical precision [25, 26, 80, 81]. Pb+Pb collisions at LHC were performed at $\sqrt{s_{\rm NN}}$ = 2.76 TeV starting from the year 2011. p+p collisions were performed at the same energy and p+Pb collisions were performed at $\sqrt{s_{\rm NN}}$ = 5.02 TeV. During second LHC run, Pb+Pb collisions were perfomed at $\sqrt{s_{\rm NN}}$ = 5.02 TeV and p+Pb collisions were perfomred at $\sqrt{s_{\rm NN}}$ = 8 TeV. The CMS experiment can reconstruct all the three states of Upsilon starting from p_T=0 covering a large central rapidity region with $|y| < 2.4$. ALICE experiment can reconstruct Upsilon in the forward rapidity range $2.5 < y < 4.0$ in muon arm. The reach of ATLAS experiment is within $|y| < 1$ but it can measure upto very high p_T. At lower energy, STAR experiment can reconstruct in mid-rapidty range $|y| < 1.0$ from zero p_T onwards.

Figure 5 shows the Υ(nS) nuclear modification factor, R_{AA} in Pb+Pb collisions at $\sqrt{s_{\rm NN}}$ = 5.02 TeV, (a) as a function of transverse momentum p_T and (b) as a function of rapidity measured by CMS [18], ALICE [82] and ATLAS experiments [82]. The vertical bars denote statistical uncertainties, and the rectangular boxes show the total systematic uncertainties. From these figures it is clear that the individual Υ states are suppressed in the Pb+Pb collisions relative to the production in the p+p collisions. One can also notice that Υ(2S) and Υ(3S) are more suppressed relative to the ground state Υ(1S) and there is se-

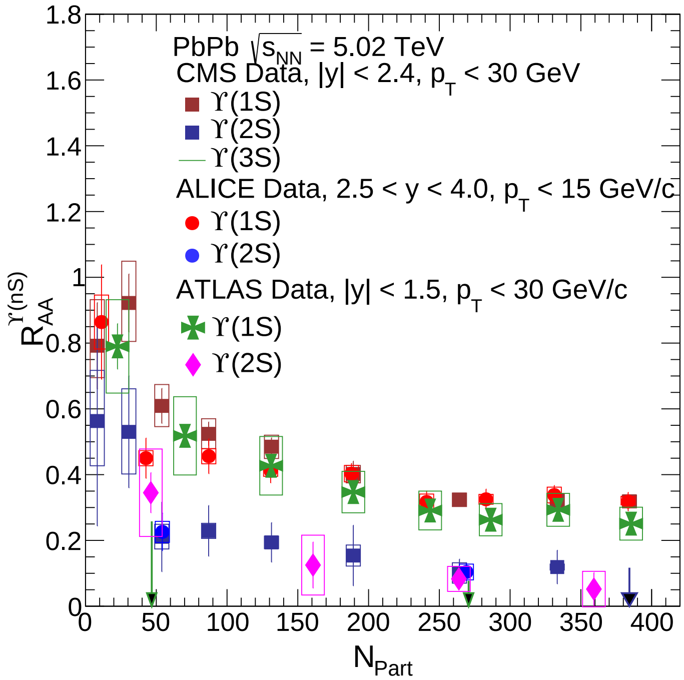

Figure 6: (Color online) The Υ(nS) nuclear modification factor, R_{AA} in Pb+Pb collisions at $\sqrt{s_{\rm NN}}$ = 5.02 TeV as a function of $N_{\rm Part}$ measured by CMS [18], ALICE experiments [82] and ATLAS experiments [82]. The vertical bars denote statistical uncertainties and the rectangular boxes show the total systematic uncertainties.

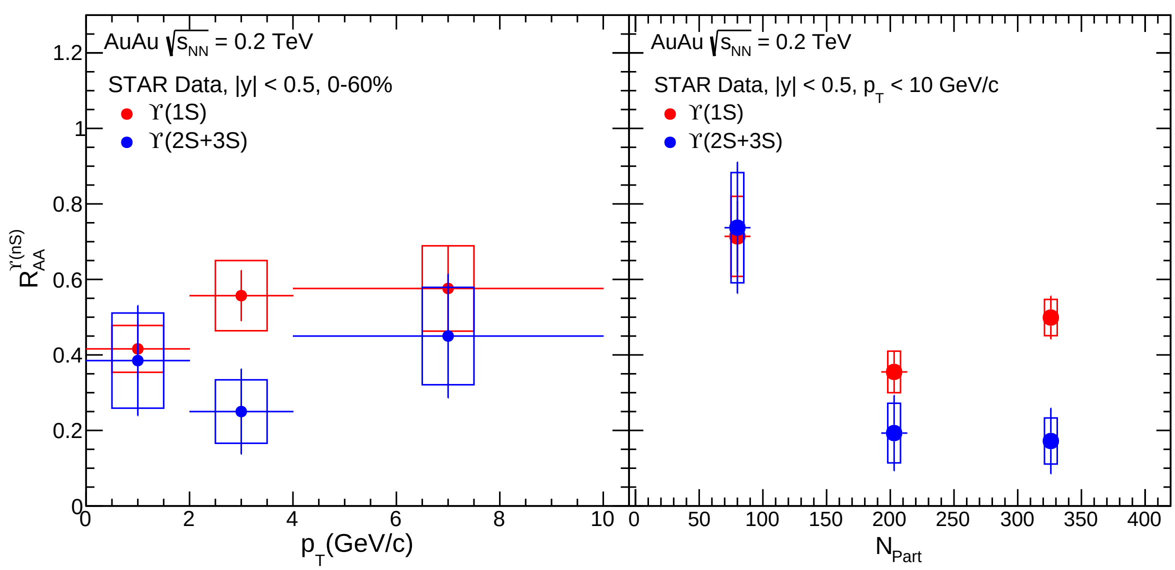

Figure 7: (Color online) The Υ(nS) nuclear modification factor, R_{AA} in Au+Au collisions at $\sqrt{s_{\rm NN}}$ = 200 GeV, (a) as a function of transverse momentum p_T and (b) as a function of $N_{\rm Part}$ measured by STAR experiments [83]. The vertical bars denote statistical uncertainties, and the rectangular boxes show the total systematic uncertainties.

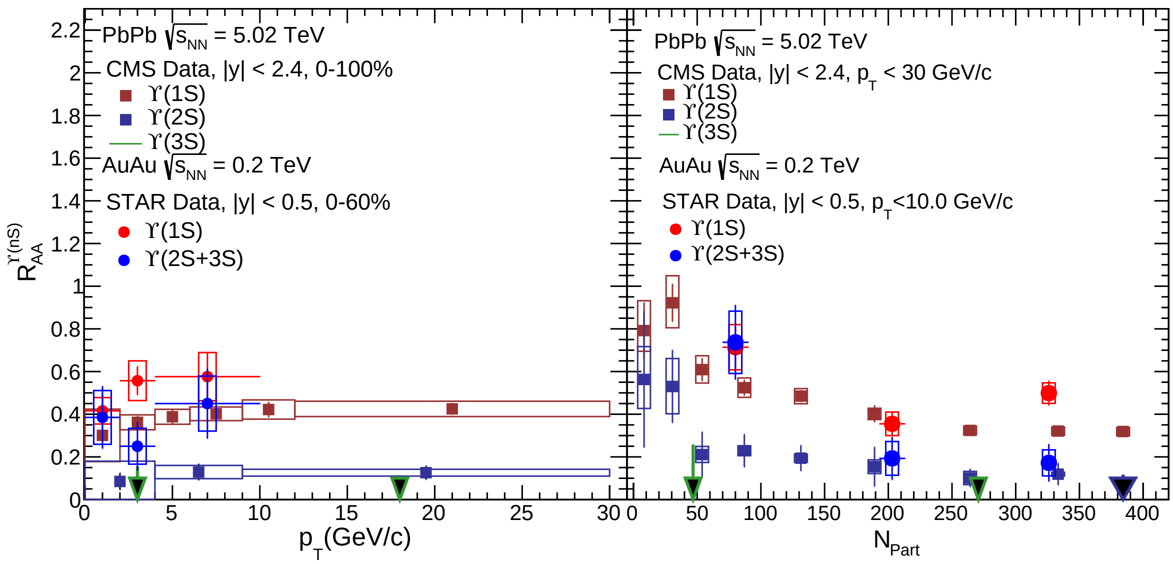

Figure 8: (Color online) The Υ(nS) nuclear modification factor, R_{AA}, (a) as a function of transverse momentum p_T and (b) as a function of $N_{\rm Part}$ measured by STAR experiments [83] at 0.2 TeV and CMS experiment [18] at 5.5 TeV. The vertical bars denote statistical uncertainties, and the rectangular boxes show the total systematic uncertainties.

quential suppression pattern as per the binding energies of the states. Υ(3S) almost disappears in Pb+Pb collisions. The suppression of Υ states increases with p_T and R_{AA} looks to be flat at high p_T although more precise measurements (at high p_T) are required to ascertain this behaviour. With increasing rapidity, the suppression remains the same and decreases slightly but only at larger rapidities. The forward rapidity $(2.5 \leq y^{\Upsilon} \leq 4.0)$ measurement of the Υ suppression at ALICE is found to be consistent with the midrapidity $(|y^{\Upsilon}| \leq 2.4)$ measurement of the Υ suppression at the CMS which again shows the weak dependence of suppression on rapidity.

Figure 6 shows the Υ(nS) nuclear modification factor, R_{AA} in Pb+Pb collisions at $\sqrt{s_{\rm NN}}$ = 5.02 TeV, as a function of $N_{\rm Part}$ measured by CMS [18], ALICE experiments [82] and ATLAS experiments [82]. The vertical bars denote statistical uncertainties and the rectangular boxes show the total systematic uncertainties. The Υ nuclear modification factor, R_{AA}, shows a strong dependence on collision centrality and the suppression of all the states increases as the collisions become more central corresponding to bigger system size. The results from different experiments seem to agree with each other although the measurements of different experiments correspond to different rapidity ranges.

Figure 7 shows the Υ(nS) nuclear modification factor, R_{AA} in Au+Au collisions at $\sqrt{s_{\rm NN}}$ = 200 GeV, (a) as a function of transverse momentum p_T and (b) as a function of $N_{\rm Part}$ measured by STAR experiments [83]. The vertical bars denote statistical uncertainties, and the rectangular boxes show the total systematic uncertainties. At RHIC energy, there is a substantial suppression of Upsilon states. Moreover,

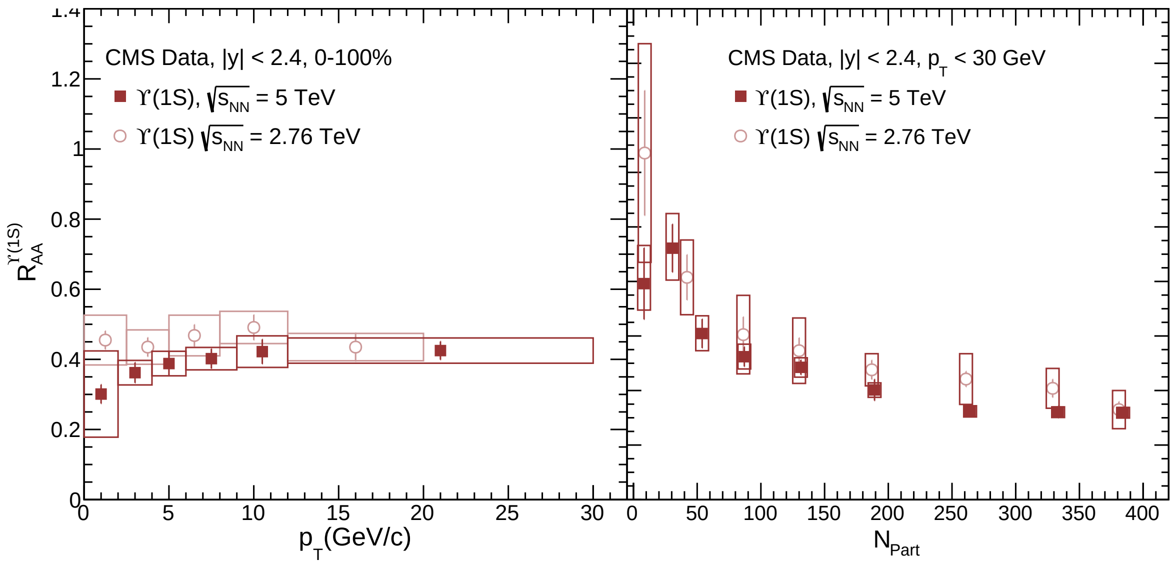

Figure 9: (Color online) The Υ(nS) nuclear modification factor, R_{AA} in Pb+Pb collisions, (a) as a function of transverse momentum p_T and (b) as a function N_{Part} measured by CMS at 2.76 [81] and 5.02 TeV [18]

the suppression pattern of Upsilon states at RHIC looks similar as we discussed for LHC; Heavier states are more suppressed, the suppression has weak dependence on p_T and strong dependence on N_{part}.

Figure 8 shows the Υ(nS) nuclear modification factor, R_{AA}, (a) as a function of transverse momentum p_T and (b) as a function of N_{Part} measured by STAR experiments [83] at $\sqrt{s_{\text{NN}}}$ =0.2 TeV and CMS experiment [18] at $\sqrt{s_{\text{NN}}}$ =5.5 TeV. The vertical bars denote statistical uncertainties, and the rectangular boxes show the total systematic uncertainties. One can note that the suppression of Upsilon states is slightly stronger at LHC as compared to that at RHIC. This is evidence of medium of increasing temperature at increasing collision energy.

Figure 9 shows the Υ(nS) nuclear modification factor, R_{AA} in Pb+Pb collisions, (a) as a function of transverse momentum p_T and (b) as a function N_{Part} measured by CMS at 2.76 [81] and 5.02 TeV [18]. The CMS experiment measured slightly more amount of Υ suppression at $\sqrt{s_{NN}}$ = 5.02 TeV than the suppression at $\sqrt{s_{NN}}$ = 2.76 TeV. The ALICE experiment on the other hand observed less suppression at $\sqrt{s_{NN}}$ = 5.02 TeV than that at $\sqrt{s_{NN}}$ = 2.76 TeV in the most central Pb+Pb collisions [20, 80].

The overall conclusions from Figures 8 and 9 is that the suppression of Upsilon states increases with collision energy albiet weakly.

To summarize, LHC provided high statistics measurements of R_{AA} in Pb+Pb collisions for all three Upsilon states over wide kinematical ranges. All Υ states are found to be suppressed in the Pb+Pb collisions, the heavier states are more suppressed relative to the ground state. The suppression of Υ states

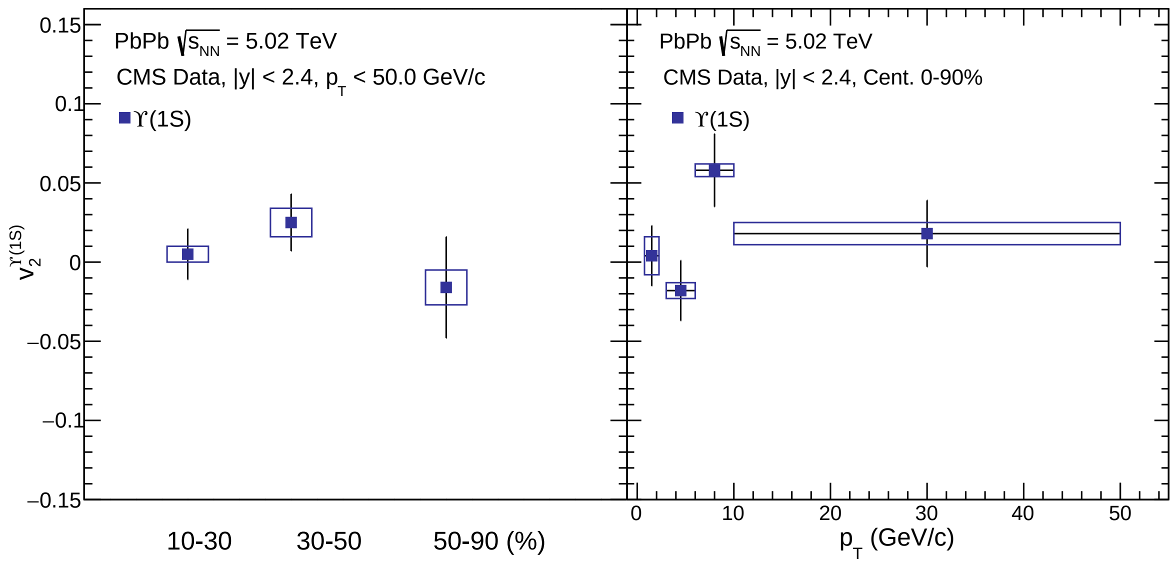

Figure 10: (Color online) The $\Upsilon(1S)$ azimuthal anisotropy (v_2) (a) as a function of collision centrality and (b) as a function of transverse momentum p_T [85]. The vertical bars denote statistical uncertainties, and the rectangular boxes show the total systematic uncertainties.

strongly depends on system size but has weak dependence on p_T and rapidity. At high p_T, more precise measurements are required to ascertain flatness in the suppression. Comparing the measurements at RHIC and at two energies of LHC, it can be said that the suppression increases with energy albiet weakly.

4.2. $\Upsilon(nS)$ Azimuthal anisotropy

In semi-central heavy ion collisions, the produced QGP has a lenticular shape in the transverse plane which is reflected in the anisotropic distribution of particles obtained using the magnitudes of the Fourier co-efficients (v_n) of the azimuthal correlation of particles [84]. By studying the azimuthal distribution of the quarkonia, it is possible to develop a more comprehensive understanding of the dynamics of their production.

The CMS experiment measured v_2 coefficients for Υ(1S) and Υ(2S) mesons in Pb+Pb collisions at $\sqrt{s_{NN}}$ = 5.02 TeV. Figure 10 shows the Υ(1S) azimuthal anisotropy (v_2) (a) as a function of collision centrality and (b) as a function of transverse momentum p_T measured by CMS experiment at LHC [85]. The p_T integrated results shown in Fig. 10 (a) for three centrality intervals are consistent with zero within the statistical uncertainties. The average v_2 values in the 10-90% centrality interval measured by CMS experiment are found to be 0.007±0.011(stat)±0.005(syst) for Υ(1S) and -0.063±0.085(stat)±0.037(syst) for Υ(2S). The p_T dependence of v_2 of Υ(1S) meson is measured for the 10-90% centrality interval. The values of v_2 are consistent with zero in the measured p_T range, except for the $6 < p_T < 10$ GeV/c interval that shows a 2.6σ deviation from zero.

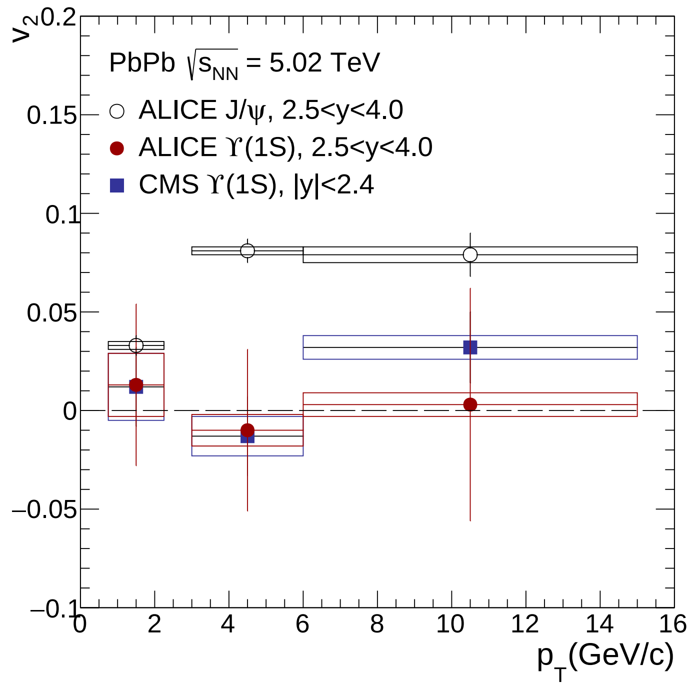

Figure 11: (Color online) The v_2 for Υ(1S) mesons as a function of p$_T$ in the rapidity range $|y| < 2.4$ measured by CMS experiment [85] compared with the ALICE results for $Upsilon$(1S) and J/ψ mesons measured in 2.5<y<4 [86]. The vertical bars denote statistical uncertainties, and the rectangular boxes show the total systematic uncertainties.

Figure 11 shows the p$_T$ differential results for v_2 of Υ(1S) mesons measured by CMS experiment along with the measurements of v_2 for Υ(1S) and J/ψ from ALICE in the same p$_T$ (0-15 GeV/c) and centrality (5-60%) interval. The measurements from CMS and ALICE are done in complementary rapidity ranges. The Υ(1S) v_2 is consistant with zero while the J/ψ meson measured by ALICE has finite v_2.

Together, the CMS and ALICE results indicate that the collective effects of the medium on the Υ(1S) are small. This also indicates that the bottom quark is not thermalized in the medium at LHC while charm quark does thermalize. It has implications for recombination yield of bottomonia at LHC.

4.3. Υ(nS) in proton Lead collisions

The nuclear modification factors and ratios of Upsilon states are measured by CMS in p+A collisions as well covering wide kinematic regions.

Figure 12 shows the Υ(nS) nuclear modification factor, R_{pA}, (a) as a function of transverse momentum p_T and (b) as a function rapidity in p+Pb colisions at $\sqrt{s_{NN}}$ = 5.02 TeV measured by CMS [87]. It is observed that all three Upsilon states are suppressed in p+Pb collisions; while R_{AA} remains flat in the measured rapidity window, it shows increasing trend with increasing p_T. The excited states are more suppressed as compared to ground state. Thus a sequential suppression pattern is vissible in p+Pb collisions

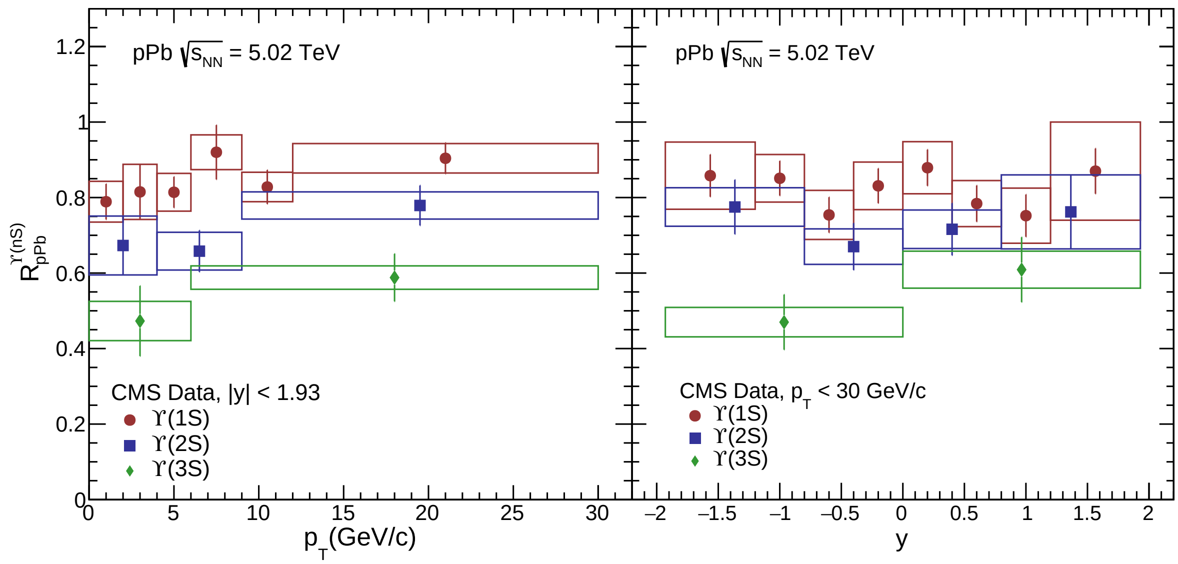

Figure 12: (Color online) The Υ(nS) nuclear modification factor, R_{pA}, (a) as a function of transverse momentum p_T and (b) as a function rapidity in p+Pb colisions at $\sqrt{s_{NN}} = 5.02$ TeV measured by CMS [87]

indcating final state effects on bottomonia production.

Figure 13 shows the Υ(nS) nuclear modification factors, R_{pA} [87] and R_{AA} [18] at $\sqrt{s_{NN}} = 5.02$ TeV measured by CMS. It is observed that Upsilon states are suppressed in both p+Pb and Pb+Pb collisions though the suppression is many times more in Pb+Pb collisions.

The CMS experiment measured the Υ ratios as a function of event activity in p+Pb collisions at $\sqrt{s_{NN}}$=5.02 TeV [88]. The results were compared with p+p and Pb+Pb collisions at $\sqrt{s}$=2.76 TeV. The nuclear modification of all Υ states is also measured in p+Pb collisions at $\sqrt{s_{\rm NN}}$ = 5.02 TeV [87]. Recently, relative production of Υ(nS) states are measured as a function of event activity in proton+proton collisions at $\sqrt{s}$ = 7 TeV [89].

Figure 14(a) shows the ratio Υ(2S)/Υ(1S) as a function of event activity measured in $\sqrt{s_{NN}}$=5.02 TeV p+Pb collisions [88] and is compared with p+p and Pb+Pb Collisions at $\sqrt{s_{NN}}$=2.76 TeV. The event activity in CMS is given by number of tracks $N_{\rm tracks}^{|y|<2.4}$ within rapidity range $|y| < 2.4$. The relative suppression of excited state with the ground state indicates final state effects in p+Pb collisions. From this figure it looks like that the relative suppression of the two Upsilon states is falling steadily with the $N_{\rm tracks}$ and this indicates that there is no difference between different collision systems if they are scaled with the event activity. However because of large error bars of data specially for Pb+Pb systems, this behaviour can not be ascertained. Moreover, the energies of p+Pb and Pb+Pb systems are different.

To get a clear picture, we obtain a new diagram using various CMS data. Figure 14(b) shows the

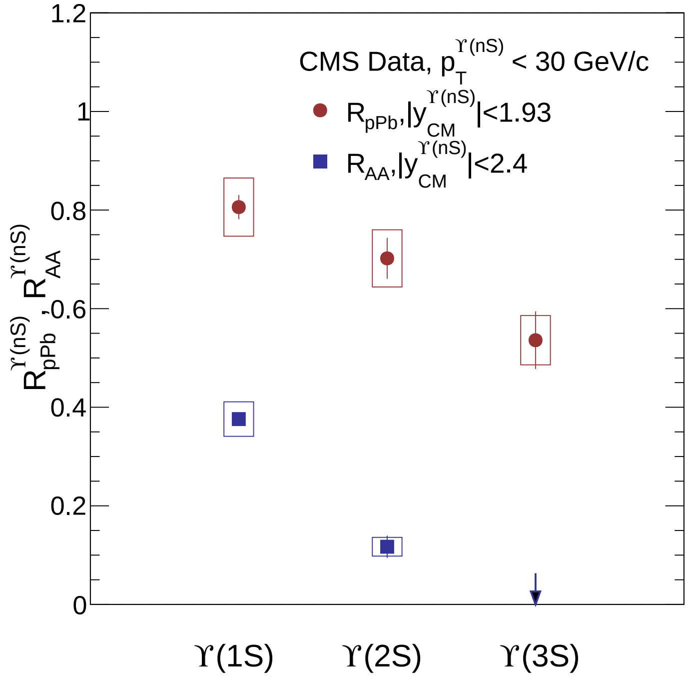

Figure 13: (Color online) The Υ(nS) nuclear modification factors, R_{pA} [87] and R_{AA} [18] at $\sqrt{s_{NN}} = 5.02$ TeV measured by CMS.

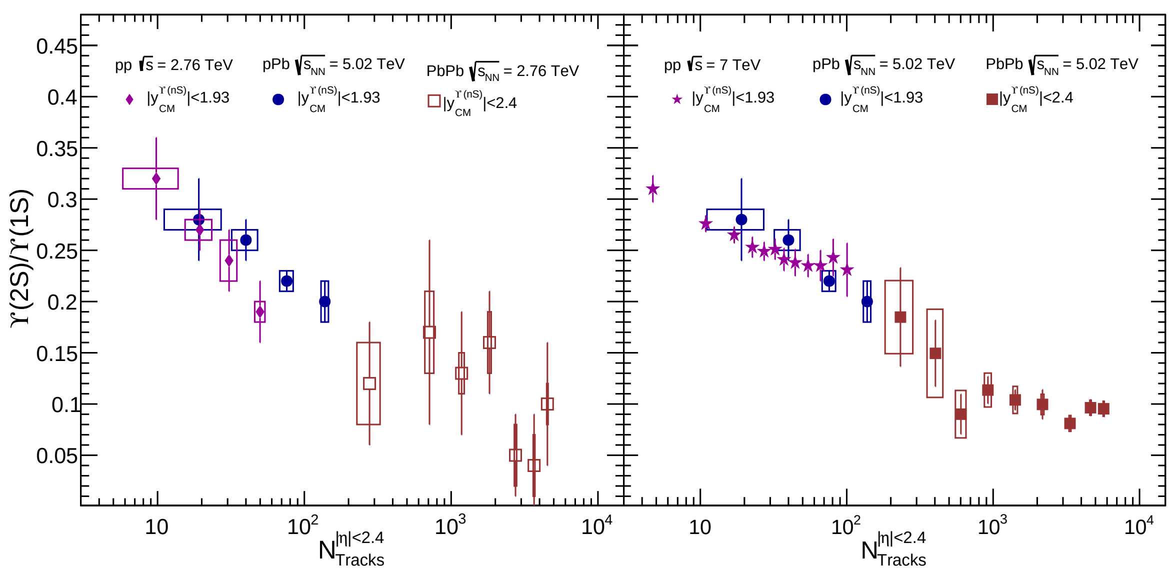

Figure 14: (Color online) (a) The ratio Υ(2S)/Υ(1S) as a function of event activity measured in $\sqrt{s_{NN}}$=5.02 TeV p+Pb collisions [88] and compared with p+p and Pb+Pb Collisions at $\sqrt{s_{NN}}$=2.76 TeV. (b) The ratio Υ(2S)/Υ(1S) as a function of event activity measured in $\sqrt{s_{NN}}$=5.02 TeV p+Pb collisions [88] and is compared with p+p collisions at $\sqrt{s}$=8 TeV [89]. The ratio of Υ(2S) and Υ(1S) in Pb+Pb Collisions at $\sqrt{s_{NN}}$=5.02 TeV has been obtained using their R_{AA} measured by CMS, the procedure explained in the text.

ratio Υ(2S)/Υ(1S) as a function of event activity measured in $\sqrt{s_{\rm NN}}$=5.02 TeV p+Pb collisions [88] and is compared with p+p collisions at $\sqrt{s}$=7 TeV [89] and Pb+Pb Collisions at $\sqrt{s_{\rm NN}}$=5.02 TeV. One can observe from this new figure that the ratio Υ(2S)/Υ(1S) decreases steadily for p+p and p+Pb systems and the peripheral Pb+Pb data also follow this pattern. Then there is a step and most central Pb+Pb data show a flatness as a function of event activity contrary to p+p and p+Pb collisions which fall steadily with increasing $N_{\rm tracks}$.

The Figure 14(b) shows the ratio of Υ(2S) and Υ(1S) in Pb+Pb Collisions at $\sqrt{s_{NN}}$=5.02 TeV which has been obtained using their $R_{\rm AA}$ measured by CMS [87]. The procedure is explained in the following. The $N_{\rm tracks}$ corresponding to $N_{\rm Part}$ at $\sqrt{s_{_{NN}}}$ = 5.02 TeV [18] can be obtained using the $N_{\rm tracks}$ for same $N_{\rm Part}$ given for 2.76 TeV [88] after scaling as

$$N_{\rm tracks}|_{5.02} = N_{\rm tracks}|_{2.76} \times \frac{dN/d\eta|_{5.02}}{dN/d\eta|_{2.76}}. \tag{9}$$

where $\frac{dN/d\eta|_{5.02}}{dN/d\eta|_{2.76}} = 1.22$ [18, 88]. The ratio Υ(2S)/Υ(1S) at $\sqrt{s_{NN}}$=5.02 can be obtained as

$$\frac{\Upsilon(2S)}{\Upsilon(1S)} = \frac{R_{AA}^{2S}}{R_{AA}^{1S}} \times \frac{\sigma_{pp}^{1S}}{\sigma_{pp}^{2S}}. \tag{10}$$

Here, σ_{pp}^{1S} and σ_{pp}^{2S} can be obtained by integrating the pp cross section measured by CMS [88] at $\sqrt{s_{_{NN}}}$ = 5.02 TeV giving $\sigma_{pp}^{1S}/\sigma_{pp}^{2S} = 0.26$.

To summarise, Upsilon states are suppressed in p+Pb collisions, although the suppression is much smaller as compared to that in p+Pb collisions. The relative suppression of excited state with the ground state indicates final state effects in p+Pb collisions. We have obtained a new figure for the ratio Υ(2S)/Υ(1S) as a function of event activity measured in p+Pb and Pb+Pb collisions at $\sqrt{s_{\rm NN}}$=5.02 TeV compared with the p+p collisions at $\sqrt{s}$=7 TeV. This study shows that the ratio Υ(2S)/Υ(1S) decreases steadily with with increasing $N_{\rm tracks}$ for p+p and p+Pb systems and the peripheral Pb+Pb data also follow the same pattern. Then there is a step and most central Pb+Pb data show a flatness as a function of event activity contrary to p+p and p+Pb collisions which fall steadily with increasing $N_{\rm tracks}$. This indicates a that the medium causing the excited states to be more suppressed in p+Pb system beahves different than that in Pb+Pb systems, the later may have been a thermalized medium and not just a system of large particles.

5. Bottomonia production mechanism in heavy ion collisions

Quarkonia are predicted to be suppressed in heavy ion collisions if QGP is formed since the force between the quarks will be colour screened in QGP phase [6]. However, very soon it was realized that the picture was not that simple. There are many factors which affect the production of quarkonia in A+A collisions. In fact, in proton-nucleus (p+A) collisions also the quarkonium suppression was observed. That part of the nucleus-nucleus suppression is due to cold-nuclear-matter (CNM) effects. Therefore it is necessary to disentangle hot and cold-medium effects. The CNM effects can arise at the initial state and/or the final state. The initial state effect arises due to modification of parton distribution functions (PDF) inside the nucleus compared to the same inside the protons. The final state modification arises due to the fact the produced quarkonia would interact with the medium leading to the destabilisation of the bound state. Furthermore, the suppression of quarkonia is thought to be of sequential in nature. The sequential suppression happens as a result of the differences of the binding energy of different bound states. The strongly bound states, such as the $\Upsilon(1\mathrm{S})$ or the J/ψ , melt at higher temperatures. On the other hand more loosely bound staes $\psi(2\mathrm{S})$, χ_c , χ_b , $\Upsilon(2\mathrm{S})$ or $\Upsilon(3\mathrm{S})$ melt at much lower temperatures. This behaviour helps estimating the initial temperature reached in the collisions [90]. However, the prediction of a sequential suppression pattern gets complicated due to feed-down decays of higher-mass resonances. The production process is further enriched, in the high energy scenario (like LHC), due to recombination process. At very high energies, abundant production of Q and $\bar{Q}$ may lead to new quarkonia production in the medium. The recombination process is more justified for charmonia state and for the bottommonia states the contribution of this process is expected to be much smaller since the bottom quark mass ($\sim$ 4.5 GeV) is three times more than the charm quark and thus its thermalization at temperatures reached at LHC ($\sim$ 0.6 GeV) will be negligible.

5.1. Cold nuclear matter effects

The baseline for quarkonium production and suppression in heavy-ion collisions should be determined from studies of cold-nuclear-matter (CNM) effects. The name cold matter arises because these effects are observed in hadron-nucleus interactions where dense matter effects are much more important compared to the hot matter. The most important CNM affect is due to the modifications of the parton distribution functions (PDF) in the nucleus compared to that in the nucleon. It depends mainly on two parameters, the momentum fraction of the parton (x) and the scale of the parton-parton interaction (Q^2). The nuclear density modified parton distribution function is known as nPDF and nPDF to PDF ratio, $R_i(x,Q^2) = f_i^{p\epsilon A}(x,Q^2)/f_i^p(x,Q^2)$ quantifies the modification due to nuclear effect. In the small x regime $(x < 10^{-2})$, this ratio is less than unity and is referred to as small-x shadowing. At intermediate $x(\sim 0.1)$ the ratio shows a hump like structure, a phenomenon known as anti-shadowing. Around $x \approx 0.6$, one observes a dip which is known as EMC effect. The dynamics of partons within the nuclei is affected by the parton saturation which is successfully studied by color glass condensate. In the final state, the quarkonia bound state scatters and re-scatters inelastically while passing through the nucleus. This leads to the breakup or absorption of the bound state which is estimated by the inelastic cross-section of the quarkonia with the nucleon.

The contributions to CNM effects look straightforward. However there are a several uncertainties associated with it. The measurement of nuclear modifications of the quark densities are relatively well-understood in nuclear deep-inelastic scattering (nDIS). On the other hand the modifications of the gluon density are not directly measured. The scaling violations in nDIS is one of the ways to constrain the nuclear gluon density. Another constraint is provided by overall momentum conservation. However, more direct probes of the gluon density are needed. The shadowing parametrizations we have in hand are derived from global fits to the nuclear parton densities. This gives wide variations in the nuclear gluon density, from almost no effect to very large shadowing at low-x, compensated by strong antishadowing around $x \sim 0.1$.

The nuclear absorption survival probability depends on the absorption cross section of the quarkonium. There are more inherent uncertainties in absorption than in the shadowing parametrization. Typically an absorption cross section is a fit to the A dependence of quarkonium production in pA collision at a given energy. This is rather simplistic since it is not known whether the object traversing the nucleus is a precursor color-octet state or a fully-formed color-singlet quarkonium state. The J/ψ absorption cross section at $y \sim 0$ is seen to decrease with energy, regardless of the chosen shadowing parametrization [91].

The analyses of J/ψ production in fixed-target interactions [91] show that the effective absorption cross section depends on the energy of the initial beam and the rapidity or x_F of the observed J/ψ . One possible interpretation is that low-momentum color-singlet states can hadronize in the target, resulting in larger effective absorption cross sections at lower center-of-mass energies and backward x_F (or center-of-mass rapidity). At higher energies, the states traverse the target more rapidly so that the x_F values at which they can hadronize in the target move back from midrapidity toward more negative x_F. Finally, at sufficiently high energies, the quarkonium states pass through the target before hadronizing, resulting in negligible absorption effects. Thus the *effective* absorption cross section decreases with increasing center-of-mass energy. This is because of the fact that faster states are less likely to hadronize inside the target.

This is a very simplistic picture. In practice, cold-nuclear-matter effects (initial-state energy loss, shadowing, final-state breakup, *etc.*) depend differently on the quarkonium kinematic variables and the collision energy. It is clearly unsatisfactory to combine all these mechanisms into an *effective* absorption cross section, as employed in the Glauber formalism, that only evaluates final-state absorption. A better understanding of absorption requires more detailed knowledge of the production mechanisms which are not fully understood yet.

The nuclear modification factors and ratios of Upsilon states are measured by CMS experiment covering wide kinematic regions. In section 4.3, Figure 12 shows the Υ(nS) nuclear modification factor, R_{pA}, as a function of transverse momentum p_T and rapidity in p+Pb colisions at 5.02 TeV measured by CMS [87]. It is observed that all three Upsilon states are suppressed in p+Pb collisions. Moreover, it is noticed that the excited states are more suppressed as compared to the ground state. Since the shadowing effects are expected to be similar on all the three states the measurements indicate final state effects on the Upsilon states which need to be understood.

5.2. *Quarkonium in hot medium*

It has been argued that the color screening in a deconfined QCD medium will destroy $Q\overline{Q}$ bound states at sufficiently high temperatures. If the binding radius of the heavy quark bound state is much greater than the screening radius, then one heavy quark gets screened from the other and the pair is broken [92]. As the temperature increases, the screening radius becomes smaller and smaller compared to the binding radius and the quarkonium states become more and more unstable. Although, this idea was proposed long ago, first principle QCD calculations, which go beyond qualitative arguments, have been performed quite recently. Such calculations include lattice QCD determinations of quarkonium correlators [93, 94, 95, 96, 97], potential model calculations of the quarkonium spectral functions with potentials based on lattice QCD [90, 98, 99, 100, 101, 102, 103, 104], also effective field theory approaches which justify potential models and reveal new medium effects [105, 106, 107, 108]. Furthermore, better modeling of quarkonium production in the medium created by heavy-ion collisions has been achieved. These new advancements make it possible to disentangle the cold and hot-medium effects on the quarkonium states which is crucial for the interpretation of heavy-ion data.

In Lattice Gauge Theory color screening is studied by calculating the spatial correlation function of a static quark and antiquark in a color-singlet state which propagates in Euclidean time from $\tau = 0$ to $\tau = 1/T$, where T is the temperature. The result of such calculations in the Lattice with dynamical quarks have been reported in Refs. [109, 110, 111]. The logarithm of the singlet correlation function, also called the singlet free energy, is shown for (2+1) flavour in Fig. 15. As expected, in the zero-temperature limit,

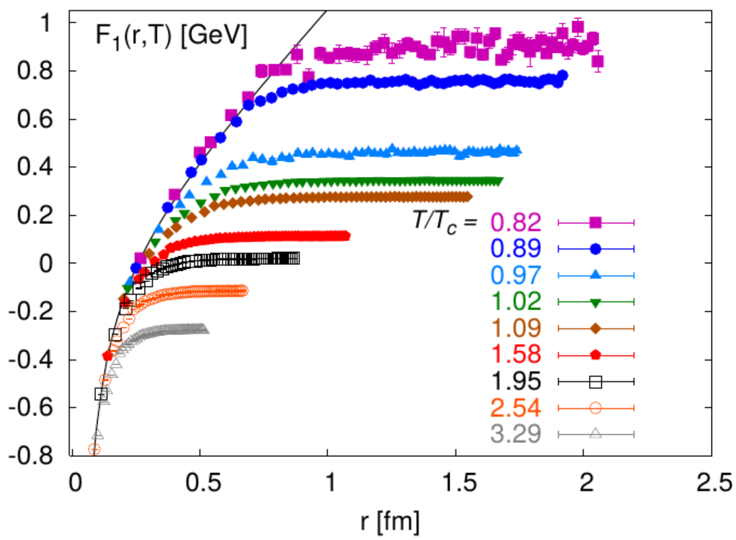

Figure 15: (Color online) The singlet free energy versus quark separation calculated in 2+1 flavour QCD on $16^3 \times 4$ lattices at different temperatures [109, 110].

the singlet free energy coincides with the zero-temperature potential. Figure 15 also illustrates that, at sufficiently short distances, the singlet free energy is temperature independent and is equal to the zero-temperature potential. The range of interaction decreases with increasing temperature. For temperatures just above the transition temperature, T_c, the heavy-quark interaction range becomes comparable to the charmonium radius. Based on this general observation, one would expect that the charmonium states, as well as the excited bottomonium states, do not remain bound at temperatures just above the deconfinement transition, often referred to as dissociation or melting.

In-medium quarkonium properties are encoded in the corresponding spectral functions, as is quarkonium dissociation at high temperatures. Spectral functions are defined as the imaginary part of the retarded correlation function of quarkonium operators. Bound states appear as peaks in the spectral functions. The peaks broaden and eventually disappear with increasing temperature which signals the melting of the given quarkonium state. The quarkonium spectral functions can be calculated in potential models using the singlet free energy from Fig. 15 or with different lattice-based potentials obtained using the singlet free energy as an input [103, 104]. The results for quenched QCD calculations are shown in Fig. 16 for S-wave charmonium and bottomonium spectral functions [103]. All charmonium states are dissolved in the deconfined phase while the bottomonium 1S state may persist up to $T \sim 2T_c$. An upper bound on the dissociation temperature (the temperatures above which no bound state peaks can be seen in the spectral function and bound state formation is suppressed) can be obtained from the analysis of the spectral functions. Conservative upper limits on the dissociation temperatures for the different quarkonium states obtained from a

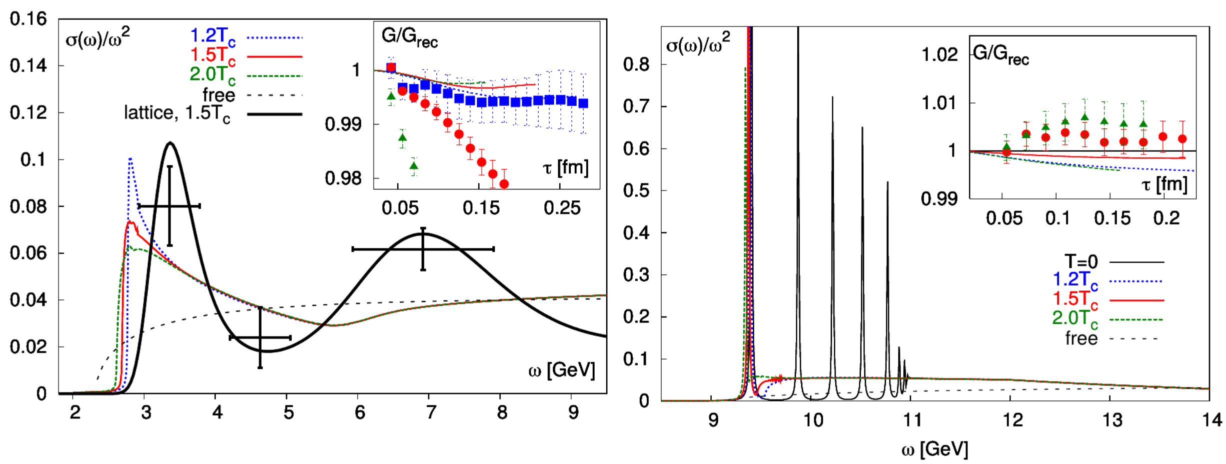

Figure 16: (Color online) The S-wave charmonium (left) and bottomonium (right) spectral functions calculated in potential models. Insets: correlators compared to lattice data. The *dotted curves* are the free spectral functions. Figures are taken from Ref. [103].

Table 7: Upper bounds on the dissociation temperatures for different quarkonia states [104].

State	$\chi_{cJ}(1P)$	$\psi^{'}$	J/ψ	$\Upsilon(2S)$	$\chi_{bJ}(1P)$	$\Upsilon(1S)$
T_{diss}	$\leq T_c$	$\leq T_c$	$1.2T_c$	$1.2T_c$	$1.3T_c$	$2T_c$

full QCD calculation [104] are given in Table 7.

Potential model calculations based on lattice QCD and resummed perturbative QCD calculations conclude that all charmonium states and the excited bottomonium states dissolve in the deconfined medium. This leads to the reduction of the quarkonium yields in heavy-ion collisions compared to the binary scaling of p+p collisions. Recombination and edge effects, however, will produce a nonzero yield.

5.3. Bottomonia suppression using Lattice QCD inspired potential model rates

Bottomonia suppression has been studied using first-principle calculation of the thermal widths of the states and considering momentum anisotropy of the plasma [112, 113, 114]. In this work, the phase-space distribution of gluons in the local rest frame is assumed to be

$$f(\mathbf{x}, \mathbf{p}) = f_{\text{iso}}\left(\sqrt{\mathbf{p}^2 + \xi(\mathbf{p}\cdot\mathbf{n})^2}/p_{\text{hard}}\right) \tag{11}$$

In the above equation ξ is a measure of the degree of anisotropy of the plasma given as $\xi = \frac{1}{2}\langle \mathbf{p}_\perp^2\rangle/\langle p_z^2\rangle - 1$ where p_z and $\mathbf{p}_\perp$ are the partonic longitudinal and transverse momenta in the local rest frame, respectively. In equation 11, p_{hard} is the momentum scale of the particles and can be identified with the temperature in an isotropic plasma.

An approximate form of the real perturbative heavy quark potential as a function of ξ can be written as [115] (for $N_c = 3$ and $N_f = 2$).

$$
\begin{aligned}
Re[V_{\rm pert}] &= -\alpha \exp(-\mu r)/r \\
\left(\frac{\mu}{m_D}\right)^{-4} &= 1 + \xi\left(1 + \frac{\sqrt{2}(1+\xi)^2\left(\cos(2\theta)-1\right)}{(2+\xi)^{5/2}}\right)
\end{aligned}
\tag{12}
$$

where $\alpha = 4\alpha_s/3$, $m_D^2 = (1.4)^2 16\pi\alpha_s\, p_{\rm hard}^2/3$ is the isotropic Debye mass and θ is the angle with respect to the beamline. The factor of $(1.4)^2$ accounts for higher-order corrections to the isotropic Debye mass [116].

This perturbative potential, given in equation (12) is modified to include the non-perturbative (long range) contributions. The modified real part of the potential is given as [115]

$$
Re[V] = -\frac{\alpha}{r}\,(1+\mu\, r)\exp\left(-\mu\, r\right) + \frac{2\sigma}{\mu}\left[1-\exp\left(-\mu\, r\right)\right] - \sigma\, r\, \exp(-\mu\, r) - \frac{0.8\,\sigma}{m_Q^2\, r}\,, \tag{13}
$$

where the last term is a temperature- and spin-independent quark mass correction [117] and $\sigma = 0.223$ GeV is the string tension. Here α is chosen to be 0.385 to match zero temperature binding energy data for heavy quark states [115]. The imaginary part of the potential is taken same as the perturbative heavy quark potential up to linear order in ξ

$$
Im[V_{\rm pert}] = -\alpha p_{\rm hard}\bigg\{\phi(\hat{r}) - \xi\left[\psi_1(\hat{r},\theta) + \psi_2(\hat{r},\theta)\right]\bigg\}, \tag{14}
$$

where $\hat{r} = m_D r$ and ϕ, ψ_1, and ψ_2 are defined in Ref. [113].

The full model potential, given by $V = Re[V] + iIm[V]$, is used to solve the Schrödinger equation. Solution of the Schrödinger equation gives the real and imaginary parts of the binding energy of the states. The imaginary part defines the instantaneous width of the state $Im[E_{\rm bind}(p_{\rm hard},\xi)] \equiv -\Gamma_T(p_{\rm hard},\xi)/2$. The resulting width $\Gamma_T(\tau)$ implicitly depends on the initial temperature of the system.

The following rate equation is used to account for in-medium bottomonia state decay,

$$
\frac{dn(\tau,\mathbf{x}_\perp,\varsigma)}{d\tau} = -\Gamma(\tau,\mathbf{x}_\perp,\varsigma)n(\tau,\mathbf{x}_\perp,\varsigma), \tag{15}
$$

where $\tau = \sqrt{t^2 - z^2}$ is the longitudinal proper time, $\mathbf{x}_\perp$ is the the transverse coordinate and $\varsigma = {\rm arctanh}(z/t)$ is the the spatial rapidity. The rate of decay is computed by [112]

$$
\Gamma(\tau,\mathbf{x}_\perp,\varsigma) = \quad 2Im[E_{\rm bind}(\tau,\mathbf{x}_\perp,\varsigma)] \qquad Re[E_{\rm bind}(\tau,\mathbf{x}_\perp,\varsigma)] > 0 \tag{16}
$$

$$
= \gamma_{\rm dis} \qquad\qquad Re[E_{\rm bind}(\tau,\mathbf{x}_\perp,\varsigma)] \leq 0. \tag{17}
$$

The suppression factor R_{AA} as a function of p_T and centrality is obtained as follows

$$
R_{AA}(\mathbf{x}_\perp,p_T,\varsigma,b) = \exp(-\bar{\gamma}(\mathbf{x}_\perp,p_T,\varsigma,b)) \tag{18}
$$

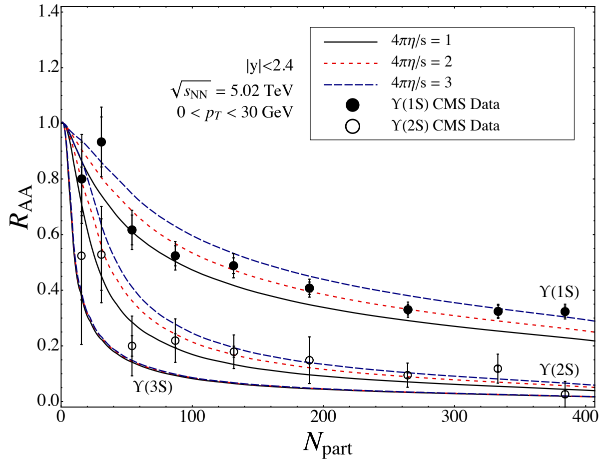

Figure 17: (Color online) Model calculations [114] of the $R_{\rm AA}$ of Υ(1S) and Υ(2S) as a function of $N_{\rm part}$ in Pb+Pb collisions at $\sqrt{s_{\rm NN}}$=5.02 TeV. A comparison is made with the data from CMS experiment [18] at the LHC.

where

$$\bar{\gamma}(\mathbf{x}_\perp, p_T, \varsigma, b) \equiv \Theta(\tau_f - \tau_{\rm form}(p_T)) \int_{\max(\tau_{\rm form}(p_T),\tau_0)}^{\tau_f} d\tau\, \Gamma_T(\tau, \mathbf{x}_\perp, \varsigma, b) \tag{19}$$

Here τ_0 and τ_f are the initial and freeze out times of the plasma and $\tau_{\rm form}$ is the formation time of the bottomonium state. Finally, one averages over $\mathbf{x}_\perp$ to obtain

$$\langle R_{AA}(p_T, \varsigma, b)\rangle \equiv \frac{\int_{\mathbf{x}_\perp} d\mathbf{x}_\perp\, T_{AA}(\mathbf{x}_\perp)\, R_{AA}(\mathbf{x}_\perp, p_T, \varsigma, b)}{\int_{\mathbf{x}_\perp} d\mathbf{x}_\perp\, T_{AA}(\mathbf{x}_\perp)} \tag{20}$$

Figure 17 shows the model calculations [114] of the $R_{\rm AA}$ of Υ(1S) and Υ(2S) as a function of $N_{\rm part}$ in Pb+Pb collisions at $\sqrt{s_{\rm NN}}$=5.02 TeV. A comparison is made with the data from CMS experiment [18] at the LHC. It is shown that there is substantial suppression of $\Upsilon(1S)$ and Υ(2S) which are attributed to the in-medium decay. A similar suppression pattern is observed for χ_{b1} which may be attributed to the finite formation time of the χ_{b1}.

5.4. *Gluon dissociation of quarkonia in dynamical medium*

The quarkonia can undergo both dissociation and recombination. The quarkonia population N_Q evolution with proper time τ can be studied via a kinetic equation [118]

$$\frac{dN_Q}{d\tau} = -\lambda_D \rho_g N_Q + \lambda_F \frac{N_{q\bar{q}}^2}{V(\tau)}, \tag{21}$$

where $V(\tau)$ is the volume of the deconfined spatial region. The λ_D is the dissociation rate obtained by the dissociation cross section averaged over the momentum distribution of gluons ρ_g and λ_F is the formation rate obtained by the formation cross section averaged over the momentum distribution of heavy quark pair q and $\bar{q}$. $N_{q\bar{q}}$ is the number of initial heavy quark pairs produced per event depending on the centrality defined by the number of participants. The number of quarkonia at freeze-out time τ_f is given by the solution of Eq. (21),

$$N_Q(p_T) = S(p_T)\, N_Q^{\rm PbPb}(p_T) + N_Q^F(p_T). \tag{22}$$

Here $N_Q^{\rm PbPb}(p_T)$ is the number of initially-produced quarkonia (including shadowing) as a function of p_T and $S(p_T)$ is their survival probability from gluon collisions at freeze-out,

$$S(p_T) = \exp\left(-\int_{\tau_0}^{\tau_f} f(\tau)\lambda_{\rm D}(T, p_T)\, \rho_g(T)\, d\tau\right). \tag{23}$$

The temperature $T(\tau)$ and the QGP fraction $f(\tau)$ evolve from initial time τ_0 to freeze-out time τ_f due to expansion of the QGP. The initial temperature and the evolution is dependent on collision centrality $N_{\rm part}$. $N_Q^F(p_T)$ is the number of regenerated quarkonia per event,

$$N_Q^F(p_T) = S(p_T) N_{q\bar{q}}^2 \int_{\tau_0}^{\tau_f} \frac{\lambda_{\rm F}(T, p_T)}{V(\tau)\, S(\tau, p_T)} d\tau. \tag{24}$$

The nuclear modification factor (R_{AA}) then can simply be written as [23, 24]

$$R_{AA}(p_T) = S(p_T)\, R(p_T) + \frac{N_Q^F(p_T)}{N_Q^{pp}(p_T)}. \tag{25}$$

Here $R(p_T)$ is the shadowing factor.

The gluon dissociation rate can be obtained in the color dipole approximation [119] as a function of gluon energy, q^0 as

$$\sigma_D(q^0) = \frac{8\pi}{3}\,\frac{16^2}{3^2}\,\frac{a_0}{m_q}\,\frac{(q^0/\epsilon_0 - 1)^{3/2}}{(q^0/\epsilon_0)^5}, \tag{26}$$

where ϵ_0 is the quarkonia binding energy and m_q is the charm/bottom quark mass and $a_0 = 1/\sqrt{m_q \epsilon_0}$. The value of ϵ_0 is equal to 1.10 GeV for Υ(1S) [120]. For the first excited state of bottomonia, Υ(2S), we use dissociation cross section from Ref. [121].

Figure 18 shows the gluon dissociation cross sections of Υ(1S) as a function of gluon energy. The dissociation cross section is zero when the gluon energy is less than the binding energy of the quarkonia. It increases with gluon energy and reaches a maximum at 1.5 GeV for $\Upsilon(1{\rm S})$. At higher gluon energies, the interaction probability decreases. We calculate the dissociation rate as a function of quarkonium momentum by integrating the dissociation cross section over thermal gluon momentum distribution $f_g(p_g)$.

We can calculate the formation cross section from the dissociation cross section using detailed balance [118, 122],

$$\sigma_F = \frac{48}{36}\,\sigma_D(q^0)\frac{(s - M_Q^2)^2}{s(s - 4m_q^2)}. \tag{27}$$

The formation rate of quarkonium with momentum **p** can be obtained using thermal distribution functions of $q/\bar{q}$.

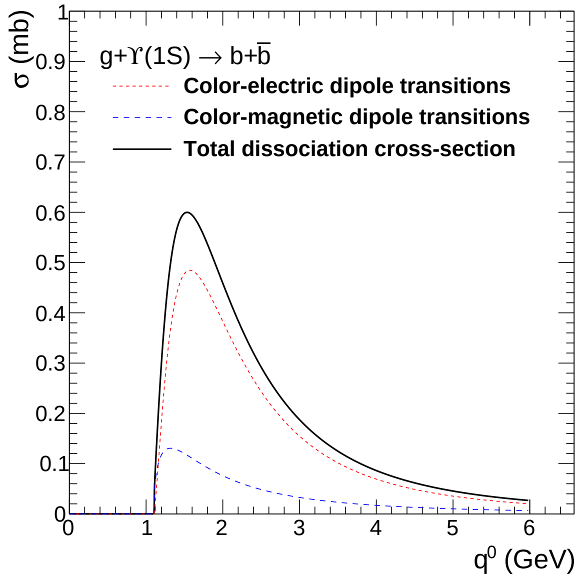

Figure 18: (Color online) Gluon dissociation cross section of Υ(1S) as a function of gluon energy (q^0) in Υ(1S) rest frame.

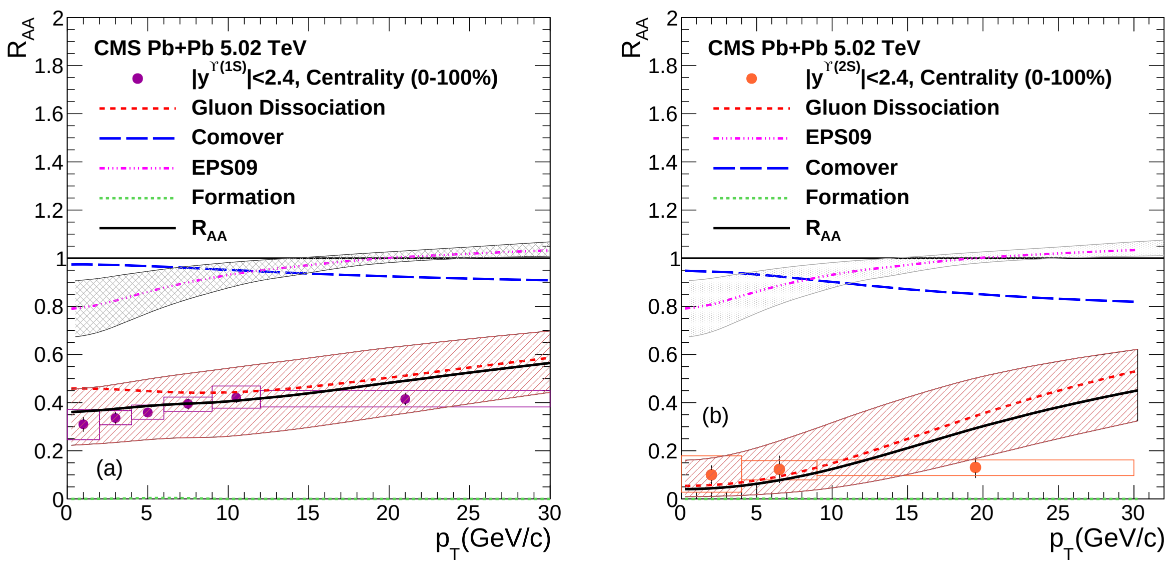

Figure 19: (Color online) Calculated nuclear modification factor (R_{AA}) [24] of (a) Υ(1S) and (b) Υ(2S) as a function of p_T compared with CMS measurements [18]. The global uncertainty in R_{AA} is shown as a band around the line at 1.

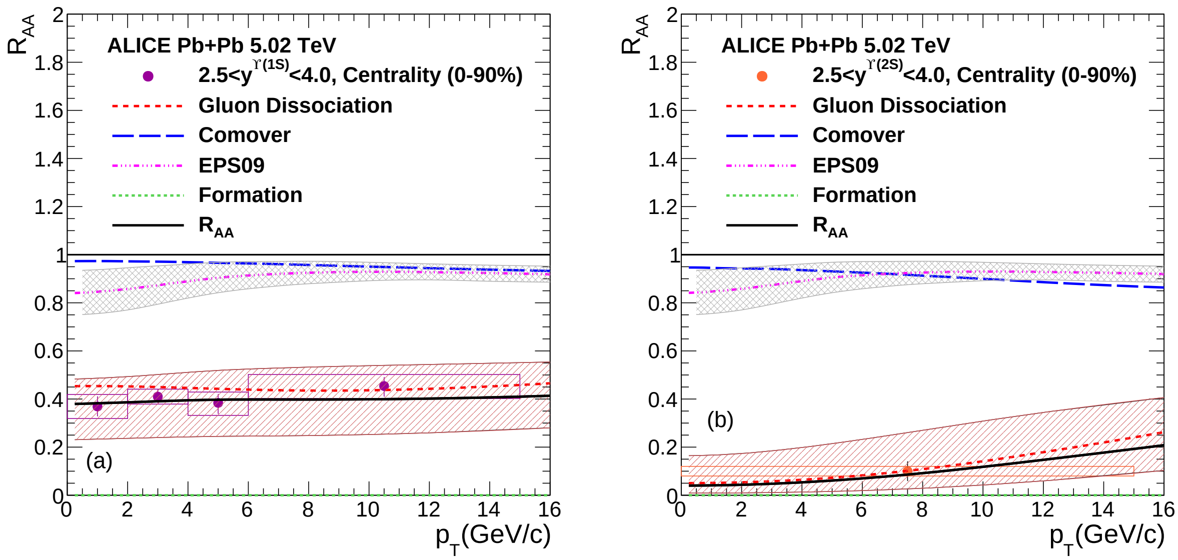

Figure 20: (Color online) Calculated nuclear modification factor (R_{AA}) [24] of (a) Υ(1S) and (b) Υ(2S) as a function of p_T in the kinematic range of ALICE detector at LHC [82]. The global uncertainty in R_{AA} is shown as a band around the line at 1.

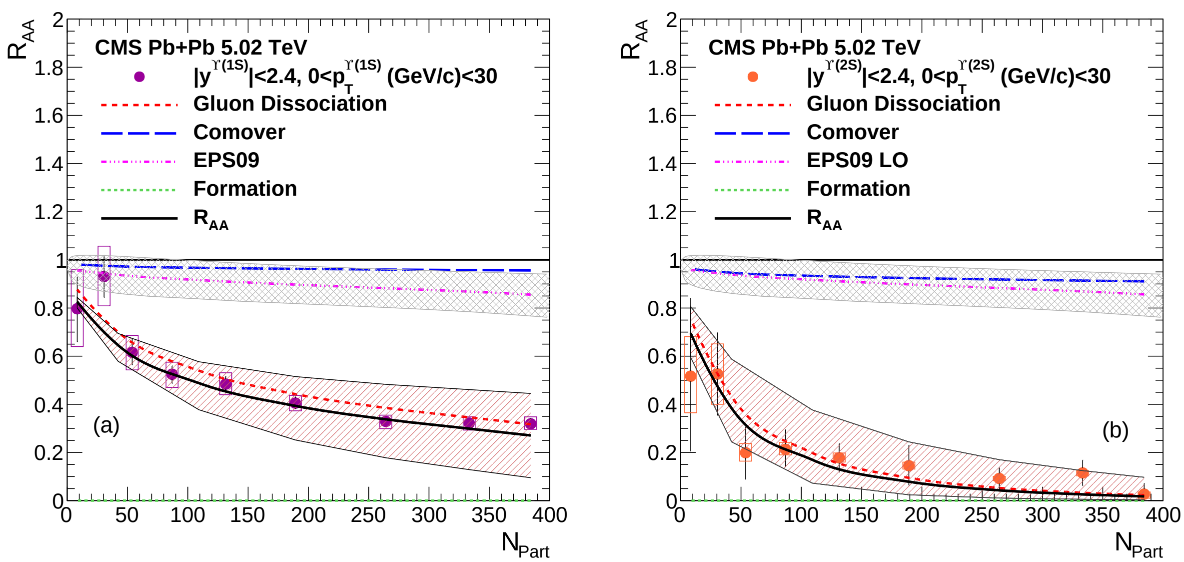

Figure 21: (Color online) Calculated nuclear modification factor (R_{AA}) [24] of (a) Υ(1S) and (b) Υ(2S) as a function of centrality of the collisions compared with the CMS measurements [18].The global uncertainty in R_{AA} is shown as a band around the line at 1.

Figure 19(a) and (b) show the calculations [24] of various contributions to the nuclear modification factor, R_{AA}, for the Υ(1S) and Υ(2S) respectively as a function of p_T compared with the mid rapidity measurements from CMS [18]. The gluon dissociation mechanism combined with the pion dissociation and shadowing corrections gives good description of data in p_T range ($p_T \approx$ 0-15 GeV/c) for both Υ(1S) and Υ(2S). The contribution from the regenerated Υs is negligible even at LHC energies. The calculations under-predict the suppression observed at the highest measured p_T for Υ(1S) and Υ(2S) which is similar for the case of J/ψ.

The feeddown corrections in the states Υ(1S) and Υ(2S) from decays of higher b$\bar{\rm b}$ bound states are obtained as

$$R_{AA}^{\Upsilon(3S)} = R_{AA}^{\Upsilon(3S)} \tag{28}$$

$$R_{AA}^{\Upsilon(2S)} = f_1 R_{AA}^{\Upsilon(2S)} + f_2 R_{AA}^{\Upsilon(3S)} \tag{29}$$

$$R_{AA}^{\Upsilon(1S)} = g_1 R_{AA}^{\Upsilon(1S)} + g_2 R_{AA}^{\chi_b(1P)} + g_3 R_{AA}^{\Upsilon(2S)} + g_4 R_{AA}^{\Upsilon(3S)} \tag{30}$$

The factors f's and g's are obtained from CDF measurement [123]. The values of g_1, g_2, g_3 and g_4 are 0.509, 0.27, 0.107 and 0.113 respectively. Here g_4 is assumed to be the combined fraction of Υ(3S) and χ_b(2P). The values of f_1 and f_2 are taken as 0.50 [112].

Figure 20(a) and (b) show the model prediction [24] of the nuclear modification factor, R_{AA}, for the Υ(1S) and Υ(2S) respectively as a function of p_T in the kinematic range covered by ALICE detector. The ALICE data [82] is well described by the model.

Figure 21(a) depicts the calculated [24] centrality dependence of the Υ(1S) nuclear modification factor, along with the midrapidity data from CMS [18]. The calculations combined with the pion dissociation and shadowing corrections gives very good description of the measured data. Figure 21(b) shows the same for the Υ(2S) along with the midrapidity CMS measurements. The suppression of the excited Υ(2S) states is also well described by the model. As stated earlier, the effect of regeneration is negligible for Υ states.

To summarise, the gluon dissociation mechanism combined with the shadowing corrections gives very good description of data in mid p_T range ($p_T \approx$ 5-10 GeV/c) for both Υ(1S) and Υ(2S). The contribution from the regenerated Υs is negligible even at LHC energies. The calculations under-predict the suppression observed at the highest measured p_T for Υ(1S) and Υ(2S) which is similar for the case of J/ψ.

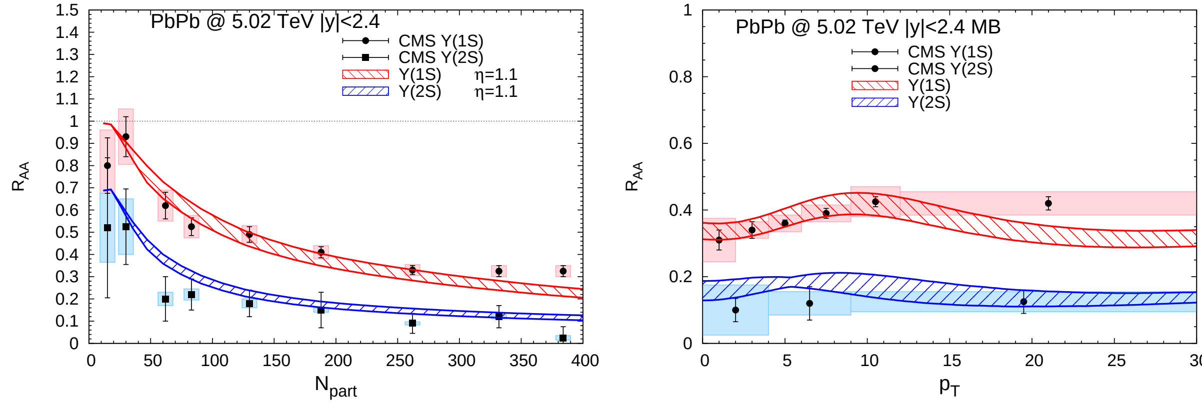

Figure 22: (Color online) Centrality (left) and transverse-momentum (right) dependence of the $R_{\rm AA}$ [127] for $\Upsilon(1S)$ and $\Upsilon(2S)$ in 5.02 TeV Pb-Pb collisions at the LHC, compared to CMS data [129]. The bands represent a 0-15 % shadowing [53] on open-bottom and bottomonia.

The suppression of quarkonia by comoving pions can be calculated by folding the quarkonium-pion dissociation cross section $\sigma_{\pi Q}$ over thermal pion distributions [124]. It is expected that at LHC energies, the comover cross section will be small [91]. The pion-quarkonia cross section is calculated by convoluting the gluon-quarkonia cross section σ_D over the gluon distribution inside the pion [121],

$$\sigma_{\pi Q}(p_\pi) = \frac{p_+^2}{2(p_\pi^2 - m_\pi^2)} \int_0^1 dx\, G(x)\, \sigma_D(xp_+/\sqrt{2}), \tag{31}$$

where $p_+ = (p_\pi + \sqrt{p_\pi^2 - m_\pi^2})/\sqrt{2}$. The gluon distribution, $G(x)$, inside a pion is given by the GRV parameterization [125]. The dissociation rate λ_{D_π} can be obtained using the thermal pion distribution.

5.5. *Transport approach for bottomonia in the medium*

The studies in Refs. [126, 127] use transport approach for the bottomomia production in the medium [126, 127]. The rate equation for bottomonium evolution in the medium's rest frame can be written as,

$$\frac{\mathrm{d}N_Y(\tau)}{\mathrm{d}\tau} = -\Gamma_Y(T)\left[N_Y(\tau) - N_Y^{\rm eq}(T)\right] \ , \tag{32}$$

Here Γ_Y, is the inelastic reaction rate and $N_Y^{\rm eq}(T)$ is the thermal equilibrium limit for each state $Y = \Upsilon(1S), \Upsilon(2S), \chi_c$. In the reaction rates both gluo-dissociation and quasi-free mechanisms have been incorporated. An important ingredient in this calculation is the bottomonium binding energies. The thermal-equilibrium limit is evaluated from the statistical model with bottom quarks [128]. The initial conditions are obtained from the p+p collision data. With these inputs, the study is carried out in a hydrodynamicaly expanding scenario.

Figure 22 shows the Centrality (left) and transverse-momentum (right) dependence of the $R_{\rm AA}$ calculated by model in Ref [127] for $\Upsilon(1S)$ and $\Upsilon(2S)$ in 5.02 TeV Pb-Pb collisions at the LHC, compared to CMS data [129]. The authors of this model found a reasonable agreement with experimental data for the centrality dependence of both $\Upsilon(1S)$ and $\Upsilon(2S)$ at both collision energies. Interestingly, they could reproduce the strong suppression of the $\Upsilon(2S)$ observed by STAR. The calculated p_T spectra at 5.02 TeV appear to capture the rather flat shapes in the CMS data at high p_T.

6. Summary and Conclusions

In this writeup we have reviewed the field of bottomonia production in p+p, p+A and A+A collisions. With immense experimental and theoretical actvities specially due to LHC measurements, many features of the bottomonia production and their behaviour in medium are well undersood.

In section 2, we have reviewed the experimental status of the bottomonia production in p+p collisions. The measurements at Tevatron, by CDF and D0 collaborations, have been discussed. The measurements at LHC, by CMS and ATLAS, at $\sqrt{s}$ = 7 TeV and 13 TeV have been reviewed. There have been some measurements of Υ polarization by CDF collaboration. The CMS and LHCb data, on Υ polarizability, confirms negligible polarization. The measurements of the cross sections and polarizations have shed light on the Υ(1S, 2S, 3S) production mechanisms in p+p collisions. LHC data has substantially extended the reach of the kinematics to test the Non-Relativistic QCD (NRQCD) and other models with higher-order corrections which becomes more distinguishable with the increase of p_T,

In section 3, we have discussed theoretical models of the bottomonia production mechanism in p+p collisions. The bottomonia study in p+p involves heavy quark pair production treatable by perturbative process and the formation of bottomonia which is a non-perturbative process. For the later one has to take recourse to some effective models. We have discussed the color singlet model, the color evaporation model and the NRQCD factorisation approach. In color singlet model, it is assumed that the $Q\bar{Q}$ pair that evolves into the quarkonium is in a color-singlet state. On the other hand in the color evaporation model, it is assumed that every produced $Q\overline{Q}$ pair can evolve into a quarkonium, if it has an invariant mass that is less than the threshold for producing a pair of open-flavor heavy mesons. The probability factor of a pair evolving into quarkonium is obtained by fitting with the experiments which is supposed to be independent of collision energy. The so-called Improved CEM reproduces the tranverse momentum dependence of the quarkonium cross section at CDF and LHC energies. We also presented NRQCD model formalism in detail. The NRQCD formalism, along with color singlet state, includes the colour octet state. In this formalism the evolution probability of $Q\bar{Q}$ pair into a state of quarkonium is expressed as matrix elements of NRQCD operators expanded in terms of heavy quark velocity v. The work using NLO cross sections are discussed and LO calculations have been reproduced for Υ(ns) production in $p+p$ collision at $\sqrt{s} = 7$

and 13 TeV.

In section 4, we have presented an experimental overview of the bottomonia results in p+A and A+A collisions at RHIC and LHC. We have looked into the R_{AA} for Υ(ns) as a functions of kinematic variables p_T, y and N_{part} at different energies and by different experiments. We have also studied v_2 for these states with centrality and p_T. LHC has provided high statistics measurements of R_{AA} for Pb+Pb collisions for all three Upsilon states over wide kinematical ranges. All Υ states are found to be suppressed in the Pb+Pb collisions, the heavier states are more suppressed relative to the ground state. The suppression of Υ states strongly depends on system size but has weak dependence on p_T and rapidity. At high p_T, more precise measurements are required to ascertain flatness in the suppression. Comparing the measurements at RHIC and at two energies of LHC, it can be said that the suppression increases with energy albiet weakly.

All the three Upsilon states are suppressed in p+Pb collisions as well and the excited states are more suppressed than the ground state indicating final state effects. We have obtained a new figure for the ratio Υ(2S)/Υ(1S) as a function of event activity measured in p+Pb and Pb+Pb collisions at $\sqrt{s_{\rm NN}}$=5.02 TeV compared with the p+p collisions at $\sqrt{s}$=7 TeV. This study shows that the ratio Υ(2S)/Υ(1S) decreases steadily with with increasing $N_{\rm tracks}$ for p+p and p+Pb systems and the peripheral Pb+Pb data also follow them. Then there is a step and most central Pb+Pb data show a flatness as a function of event activity contrary to p+p and p+Pb collisions which fall steadily with increasing $N_{\rm tracks}$. This behaviour can be used to distinguish the Pb+Pb collision system with the smaller systems.

No significant v_2 is found for Υ(1S) measured by CMS experiment. This shows that the bottom quark is not thermalized in the medium. The recombination yield of bottomonia calculated using our model is very small.

In section 5 we have discussed the mechanisms for the modification of bottomonia yields in heavy ion collisions. Starting with the idea of colour screening we have discussed the more recent ideas like modification of spectral functions of quarkonia states as a function of temperature. The cold nuclear matter has been reviewed in certain amount of detail. The excited bottomonia states are more suppressed as compared to ground state, an effect which can not be produced by shadowing effect. The final state effects in p+A collisions require a better theoretical understanding. We have reviewed some if not all the theoretical models treating both the quarkonia dissociation and recombination in dynamical medium. The comparison of the theoretical results with the experiments show that the bottomonia production can be understood in terms of colour screening or gluon dissociation. There is no significant recombination is needed a picture which is also consistent with the small values of v_2 measured by the experiments.

Acknowledgement

AB thanks Partha Pratim Bhaduri for helpful discussions.

References

[1] B. Povh, K. Rith, C. Scholz, F. Zersche, W. Rodejohann, Particles and nuclei: An Introduction to the physical concepts, Graduate Texts in Physics, Springer, 1995. doi:10.1007/3-540-36684-9.

[2] S. M. Ikhdair, R. Sever, A Systematic study on nonrelativistic quarkonium interaction, Int. J. Mod. Phys. A 21 (2006) 3989–4002. arXiv:hep-ph/0508144, doi:10.1142/S0217751X06030953.

[3] E. V. Shuryak, Quantum Chromodynamics and the Theory of Superdense Matter, Phys. Rept. 61 (1980) 71–158. doi:10.1016/0370-1573(80)90105-2.

[4] H. Satz, The Quark-Gluon Plasma: A Short Introduction, Nucl. Phys. A 862-863 (2011) 4–12. arXiv:1101.3937, doi:10.1016/j.nuclphysa.2011.05.014.

[5] H. Satz, Color deconfinement in nuclear collisions, Rept. Prog. Phys. 63 (2000) 1511. arXiv:hep-ph/0007069, doi:10.1088/0034-4885/63/9/203.

[6] T. Matsui, H. Satz, J/ψ Suppression by Quark-Gluon Plasma Formation, Phys. Lett. B 178 (1986) 416–422. doi:10.1016/0370-2693(86)91404-8.

[7] L. Kluberg, 20 years of J/psi suppression at the CERN SPS: Results from experiments NA38, NA51 and NA50, Eur. Phys. J. C 43 (2005) 145–156. doi:10.1140/epjc/s2005-02245-6.

[8] F. Abe, et al., Υ production in $p\bar{p}$ collisions at $\sqrt{s}$ = 1.8 TeV, Phys. Rev. Lett. 75 (1995) 4358. doi:10.1103/PhysRevLett.75.4358.

[9] D. Acosta, et al., Υ Production and Polarization in $p\bar{p}$ Collisions at $\sqrt{s}$ = 1.8-TeV, Phys. Rev. Lett. 88 (2002) 161802. doi:10.1103/PhysRevLett.88.161802.

[10] V. M. Abazov, et al., Measurement of inclusive differential cross sections for Υ_{1S} production in $p\bar{p}$ collisions at $\sqrt{s}$ = 1.96-TeV, Phys. Rev. Lett. 94 (2005) 232001, [Erratum: Phys.Rev.Lett. 100, 049902 (2008)]. arXiv:hep-ex/0502030, doi:10.1103/PhysRevLett.94.232001.

[11] V. Khachatryan, et al., Upsilon Production Cross-Section in pp Collisions at $\sqrt{s}$=7 TeV, Phys. Rev. D 83 (2011) 112004. arXiv:1012.5545, doi:10.1103/PhysRevD.83.112004.

[12] V. Khachatryan, et al., Measurements of the Υ(1S), Υ(2S), and Υ(3S) differential cross sections in pp collisions at $\sqrt{s} = 7$ TeV, Phys. Lett. B 749 (2015) 14–34. arXiv:1501.07750, doi:10.1016/j.physletb.2015.07.037.

[13] G. Aad, et al., Measurement of Upsilon production in 7 TeV pp collisions at ATLAS, Phys. Rev. D 87 (5) (2013) 052004. arXiv:1211.7255, doi:10.1103/PhysRevD.87.052004.

[14] A. M. Sirunyan, et al., Measurement of quarkonium production cross sections in pp collisions at $\sqrt{s} = 13$ TeV, Phys. Lett. B 780 (2018) 251–272. arXiv:1710.11002, doi:10.1016/j.physletb.2018.02.033.

[15] R. Aaij, et al., Measurement of Υ production in pp collisions at $\sqrt{s}$= 13 TeV, JHEP 07 (2018) 134, [Erratum: JHEP 05, 076 (2019)]. arXiv:1804.09214, doi:10.1007/JHEP07(2018)134.

[16] A. M. Sirunyan, et al., Measurement of prompt and nonprompt charmonium suppression in PbPb collisions at 5.02 TeV, Eur. Phys. J. C 78 (6) (2018) 509. arXiv:1712.08959, doi:10.1140/epjc/s10052-018-5950-6.

[17] A. M. Sirunyan, et al., Suppression of Excited Υ States Relative to the Ground State in Pb-Pb Collisions at $\sqrt{s_{\rm NN}}$=5.02 TeV, Phys. Rev. Lett. 120 (14) (2018) 142301. arXiv:1706.05984, doi:10.1103/PhysRevLett.120.142301.

[18] A. M. Sirunyan, et al., Measurement of nuclear modification factors of Υ(1S), Υ(2S), and Υ(3S) mesons in PbPb collisions at $\sqrt{s_{_{\mathrm{NN}}}} = 5.02$ TeV, Phys. Lett. B 790 (2019) 270–293. arXiv:1805.09215, doi:10.1016/j.physletb.2019.01.006.

[19] S. Acharya, et al., Studies of J/ψ production at forward rapidity in Pb-Pb collisions at $\sqrt{s_{\rm NN}}$ = 5.02 TeV, JHEP 02 (2020) 041. arXiv:1909.03158, doi:10.1007/JHEP02(2020)041.

[20] S. Acharya, et al., Υ suppression at forward rapidity in Pb-Pb collisions at $\sqrt{s_{\rm NN}}$ = 5.02 TeV, Phys. Lett. B 790 (2019) 89–101. arXiv:1805.04387, doi:10.1016/j.physletb.2018.11.067.

[21] M. Strickland, Thermal v_{1s} and chi_b1 suppression in $\sqrt{s_{NN}} = 2.76$ TeV Pb-Pb collisions at the LHC, Phys. Rev. Lett. 107 (2011) 132301. arXiv:1106.2571, doi:10.1103/PhysRevLett.107.132301.

[22] T. Song, K. C. Han, C. M. Ko, Bottomonia suppression in heavy-ion collisions, Phys. Rev. C 85 (2012) 014902. arXiv:1109.6691, doi:10.1103/PhysRevC.85.014902.

[23] V. Kumar, P. Shukla, R. Vogt, Quarkonia suppression in PbPb collisions at $\sqrt{s_{NN}}$ = 2.76 TeV, Phys. Rev. C 92 (2) (2015) 024908. arXiv:1410.3299, doi:10.1103/PhysRevC.92.024908.

[24] V. Kumar, P. Shukla, A. Bhattacharyya, Suppression of quarkonia in PbPb collisions at $\sqrt{s_{NN}} =$ 5.02 TeV, J. Phys. G 47 (1) (2020) 015104. arXiv:1909.10785, doi:10.1088/1361-6471/ab51cf.

[25] S. Chatrchyan, et al., Indications of suppression of excited Υ states in PbPb collisions at $\sqrt{S_{NN}}$ = 2.76 TeV, Phys. Rev. Lett. 107 (2011) 052302. arXiv:1105.4894, doi:10.1103/PhysRevLett.107.052302.

[26] S. Chatrchyan, et al., Observation of Sequential Upsilon Suppression in PbPb Collisions, Phys. Rev. Lett. 109 (2012) 222301, [Erratum: Phys.Rev.Lett. 120, 199903 (2018)]. arXiv:1208.2826, doi:10.1103/PhysRevLett.109.222301.

[27] L. Adamczyk, et al., Suppression of Υ production in d+Au and Au+Au collisions at $\sqrt{s_{NN}}$=200 GeV, Phys. Lett. B 735 (2014) 127–137, [Erratum: Phys.Lett.B 743, 537–541 (2015)]. arXiv:1312.3675, doi:10.1016/j.physletb.2014.06.028.

[28] S. W. Herb, D. C. Hom, L. M. Lederman, J. C. Sens, H. D. Snyder, J. K. Yoh, J. A. Appel, B. C. Brown, C. N. Brown, W. R. Innes, K. Ueno, T. Yamanouchi, A. S. Ito, H. Jöstlein, D. M. Kaplan, R. D. Kephart, Observation of a dimuon resonance at 9.5 gev in 400-gev proton-nucleus collisions, Phys. Rev. Lett. 39 (1977) 252–255. doi:10.1103/PhysRevLett.39.252.
URL https://link.aps.org/doi/10.1103/PhysRevLett.39.252

[29] G. Aad, et al., Measurement of the $\Upsilon(1S)$ production cross-section in *pp* collisions at $\sqrt{s} = 7$ TeV in ATLAS, Phys. Lett. B 705 (2011) 9–27. arXiv:1106.5325, doi:10.1016/j.physletb.2011.09.092.

[30] S. Chatrchyan, et al., Measurement of the $\Upsilon(1S)$, $\Upsilon(2S)$, and $\Upsilon(3S)$ Cross Sections in pp Collisions at $\sqrt{s}$ = 7 TeV, Phys. Lett. B 727 (2013) 101–125. arXiv:1303.5900, doi:10.1016/j.physletb.2013.10.033.

[31] V. M. Abazov, et al., Measurement of the polarization of the $\Upsilon(1S)$ and $\Upsilon(2S)$ states in $p\bar{p}$ collisions at $\sqrt{s}$ = 1.96-TeV, Phys. Rev. Lett. 101 (2008) 182004. arXiv:0804.2799, doi:10.1103/PhysRevLett.101.182004.

[32] T. Aaltonen, et al., Measurements of Angular Distributions of Muons From Υ Meson Decays in $p\bar{p}$ Collisions at $\sqrt{s} = 1.96$ TeV, Phys. Rev. Lett. 108 (2012) 151802. arXiv:1112.1591, doi:10.1103/PhysRevLett.108.151802.

[33] S. Chatrchyan, et al., Measurement of the $Y(1S), Y(2S)$ and $Y(3S)$ Polarizations in pp Collisions at $\sqrt{s} = 7$ TeV, Phys. Rev. Lett. 110 (8) (2013) 081802. arXiv:1209.2922, doi:10.1103/PhysRevLett.110.081802.

[34] P. Nason, S. Dawson, R. K. Ellis, The One Particle Inclusive Differential Cross-Section for Heavy Quark Production in Hadronic Collisions, Nucl. Phys. B 327 (1989) 49–92, [Erratum: Nucl.Phys.B 335, 260–260 (1990)]. doi:10.1016/0550-3213(89)90286-1.

[35] G. T. Bodwin, E. Braaten, G. P. Lepage, Rigorous QCD analysis of inclusive annihilation and production of heavy quarkonium, Phys. Rev. D 51 (1995) 1125–1171, [Erratum: Phys.Rev.D 55, 5853 (1997)]. arXiv:hep-ph/9407339, doi:10.1103/PhysRevD.55.5853.

[36] N. Brambilla, et al., QCD and Strongly Coupled Gauge Theories: Challenges and Perspectives, Eur. Phys. J. C 74 (10) (2014) 2981. arXiv:1404.3723, doi:10.1140/epjc/s10052-014-2981-5.

[37] M. B. Einhorn, S. D. Ellis, Hadronic Production of the New Resonances: Probing Gluon Distributions, Phys. Rev. D 12 (1975) 2007. doi:10.1103/PhysRevD.12.2007.

[38] E. L. Berger, D. L. Jones, Inelastic Photoproduction of J/psi and Upsilon by Gluons, Phys. Rev. D 23 (1981) 1521–1530. doi:10.1103/PhysRevD.23.1521.

[39] H. Fritzsch, Producing Heavy Quark Flavors in Hadronic Collisions: A Test of Quantum Chromodynamics, Phys. Lett. B 67 (1977) 217–221. doi:10.1016/0370-2693(77)90108-3.

[40] J. F. Amundson, O. J. P. Eboli, E. M. Gregores, F. Halzen, Colorless states in perturbative QCD: Charmonium and rapidity gaps, Phys. Lett. B 372 (1996) 127–132. arXiv:hep-ph/9512248, doi:10.1016/0370-2693(96)00035-4.

[41] P. Nason, S. Dawson, R. K. Ellis, The Total Cross-Section for the Production of Heavy Quarks in Hadronic Collisions, Nucl. Phys. B 303 (1988) 607–633. doi:10.1016/0550-3213(88)90422-1.

[42] N. Brambilla, et al., Heavy quarkonium physicsarXiv:hep-ph/0412158, doi:10.5170/CERN-2005-005.

[43] S. D. Ellis, M. B. Einhorn, C. Quigg, Comment on Hadronic Production of Psions, Phys. Rev. Lett. 36 (1976) 1263. doi:10.1103/PhysRevLett.36.1263.

[44] C. E. Carlson, R. Suaya, Hadronic Production of psi/J Mesons, Phys. Rev. D 14 (1976) 3115. doi:10.1103/PhysRevD.14.3115.

[45] G. A. Schuler, Quarkonium production and decays, Ph.D. thesis, Hamburg U. (1994). arXiv:hep-ph/9403387.

[46] P. Artoisenet, J. P. Lansberg, F. Maltoni, Hadroproduction of J/ψ and Υ in association with a heavy-quark pair, Phys. Lett. B 653 (2007) 60–66. arXiv:hep-ph/0703129, doi:10.1016/j.physletb.2007.04.031.

[47] J. M. Campbell, F. Maltoni, F. Tramontano, QCD corrections to J/psi and Upsilon production at hadron colliders, Phys. Rev. Lett. 98 (2007) 252002. arXiv:hep-ph/0703113, doi:10.1103/PhysRevLett.98.252002.

[48] P. Artoisenet, J. M. Campbell, J. P. Lansberg, F. Maltoni, F. Tramontano, Υ Production at Fermilab Tevatron and LHC Energies, Phys. Rev. Lett. 101 (2008) 152001. arXiv:0806.3282, doi:10.1103/PhysRevLett.101.152001.

[49] J. F. Amundson, O. J. P. Eboli, E. M. Gregores, F. Halzen, Quantitative tests of color evaporation: Charmonium production, Phys. Lett. B 390 (1997) 323–328. arXiv:hep-ph/9605295, doi:10.1016/S0370-2693(96)01417-7.

[50] R. E. Nelson, R. Vogt, A. D. Frawley, Narrowing the uncertainty on the total charm cross section and its effect on the J/ψ cross section, Phys. Rev. C 87 (1) (2013) 014908. arXiv:1210.4610, doi:10.1103/PhysRevC.87.014908.

[51] V. Kumar, P. Shukla, R. Vogt, Components of the dilepton continuum in Pb+Pb collisions at $\sqrt{s_{_{NN}}} =$ 2.76 TeV, Phys. Rev. C 86 (2012) 054907. arXiv:1205.3860, doi:10.1103/PhysRevC.86.054907.

[52] H.-L. Lai, J. Guzzi, Marco an dHuston, Z. Li, P. M. Nadolsky, J. Pumplin, C. P. Yuan, New parton distributions for collider physics, Phys. Rev. DarXiv:1007.2241, doi:10.1103/PhysRevD.82.074024.

[53] K. J. Eskola, H. Paukkunen, C. A. Salgado, EPS09: A New Generation of NLO and LO Nuclear Parton Distribution Functions, JHEP 04 (2009) 065. arXiv:0902.4154, doi:10.1088/1126-6708/2009/04/065.

[54] S. Chatrchyan, et al., Observation and studies of jet quenching in PbPb collisions at nucleon-nucleon center-of-mass energy = 2.76 TeV, Phys. Rev. C 84 (2011) 024906. arXiv:1102.1957, doi:10.1103/PhysRevC.84.024906.

[55] V. Cheung, R. Vogt, Production and polarization of prompt $\Upsilon(n\mathrm{S})$ in the improved color evaporation model using the k_T-factorization approach, Phys. Rev. D 99 (3) (2019) 034007. arXiv:1811.11570, doi:10.1103/PhysRevD.99.034007.

[56] J. L. Domenech, M. A. Sanchis-Lozano, Bottomonium production at the Tevatron and the LHC, Phys. Lett. B 476 (2000) 65–72. arXiv:hep-ph/9911332, doi:10.1016/S0370-2693(00)00119-2.

[57] J. L. Domenech, M. A. Sanchis-Lozano, Results from bottomonia production at the Tevatron and prospects for the LHC, Nucl. Phys. B 601 (2001) 395–421. arXiv:hep-ph/0012296, doi:10.1016/S0550-3213(01)00053-0.

[58] E. Braaten, S. Fleming, A. K. Leibovich, NRQCD analysis of bottomonium production at the Tevatron, Phys. Rev. D 63 (2001) 094006. arXiv:hep-ph/0008091, doi:10.1103/PhysRevD.63.094006.

[59] B. Gong, J.-X. Wang, H.-F. Zhang, QCD corrections to Υ production via color-octet states at the Tevatron and LHC, Phys. Rev. D 83 (2011) 114021. arXiv:1009.3839, doi:10.1103/PhysRevD.83.114021.

[60] R. Sharma, I. Vitev, High transverse momentum quarkonium production and dissociation in heavy ion collisions, Phys. Rev. C 87 (4) (2013) 044905. arXiv:1203.0329, doi:10.1103/PhysRevC.87.044905.

[61] B. Gong, L.-P. Wan, J.-X. Wang, H.-F. Zhang, Complete next-to-leading-order study on the yield and polarization of $\Upsilon(1S, 2S, 3S)$ at the Tevatron and LHC, Phys. Rev. Lett. 112 (3) (2014) 032001. arXiv:1305.0748, doi:10.1103/PhysRevLett.112.032001.

[62] Y. Feng, B. Gong, L.-P. Wan, J.-X. Wang, An updated study of Υ production and polarization at the Tevatron and LHC, Chin. Phys. C 39 (12) (2015) 123102. arXiv:1503.08439, doi:10.1088/1674-1137/39/12/123102.

[63] H. Han, Y.-Q. Ma, C. Meng, H.-S. Shao, Y.-J. Zhang, K.-T. Chao, $\Upsilon(nS)$ and $\chi_b(nP)$ production at hadron colliders in nonrelativistic QCD, Phys. Rev. D 94 (1) (2016) 014028. arXiv:1410.8537, doi:10.1103/PhysRevD.94.014028.

[64] G.-M. Yu, Y.-B. Cai, Y.-D. Li, J.-S. Wang, Heavy quarkonium photoproduction in ultrarelativistic heavy ion collisions, Phys. Rev. C 95 (1) (2017) 014905, [Addendum: Phys.Rev.C 95, 069901 (2017)]. arXiv:1703.03194, doi:10.1103/PhysRevC.95.014905.

[65] V. Kumar, K. Saha, P. Shukla, A. Bhattacharyya, Bottomonia production in p + p collisions under NRQCD formalism, Nucl. Phys. A 1013 (2021) 122226. arXiv:2106.00940, doi:10.1016/j.nuclphysa.2021.122226.

[66] D. Acosta, et al., Υ Production and Polarization in $p\bar{p}$ Collisions at $\sqrt{s} = 1.8$-TeV, Phys. Rev. Lett. 88 (2002) 161802. doi:10.1103/PhysRevLett.88.161802.

[67] R. Aaij, et al., Measurement of Upsilon production in pp collisions at $\sqrt{s}$ = 7 TeV, Eur. Phys. J. C 72 (2012) 2025. arXiv:1202.6579, doi:10.1140/epjc/s10052-012-2025-y.

[68] V. Kumar, P. Shukla, Charmonia production in p + p collisions under NRQCD formalism, J. Phys. G 44 (8) (2017) 085003. arXiv:1606.08265, doi:10.1088/1361-6471/aa7818.

[69] R. Baier, R. Ruckl, Hadronic Collisions: A Quarkonium Factory, Z. Phys. C 19 (1983) 251. doi:10.1007/BF01572254.

[70] B. Humpert, NARROW HEAVY RESONANCE PRODUCTION BY GLUONS, Phys. Lett. B 184 (1987) 105–107. doi:10.1016/0370-2693(87)90496-5.

[71] R. Gastmans, W. Troost, T. T. Wu, Production of Heavy Quarkonia From Gluons, Nucl. Phys. B 291 (1987) 731. doi:10.1016/0550-3213(87)90493-7.

[72] P. L. Cho, A. K. Leibovich, Color octet quarkonia production, Phys. Rev. D 53 (1996) 150–162. arXiv:hep-ph/9505329, doi:10.1103/PhysRevD.53.150.

[73] P. L. Cho, A. K. Leibovich, Color octet quarkonia production. 2., Phys. Rev. D 53 (1996) 6203–6217. arXiv:hep-ph/9511315, doi:10.1103/PhysRevD.53.6203.

[74] T.-J. Hou, et al., New CTEQ global analysis of quantum chromodynamics with high-precision data from the LHC, Phys. Rev. D 103 (1) (2021) 014013. arXiv:1912.10053, doi:10.1103/PhysRevD.103.014013.

[75] E. Braaten, T. Yuan, Gluon Fragmentation into Heavy Quarkonium, Phys. Rev. Lett. 71 (1993) 1673. arXiv:hep-ph/9303205, doi:https://journals.aps.org/prl/abstract/10.1103/PhysRevLett.71.1673.

[76] K. Sridhar, Quarkonium production via fragmentation: A ReviewarXiv:hep-ph/9511433.

[77] S. P. Baranov, Topics in associated J/ψ $\rightarrow$ c $\bar{c}$ production at modern colliders., Phys. Rev. D 73 (2006) 074021.

[78] S. P. Baranov, Associated $\Upsilon + b + \bar{b}$ production at the Fermilab Tevatron and ERN LHC, Phys. Rev. D 74 (2006) 074021.

[79] S. P. Baranov, A. P. Lipatov, N. P. Zotov, Prompt J/ψ production at LHC: new evidence for the k_T-factorization, Phys. Rev. D 85 (2012) 014034. arXiv:1108.2856, doi:https://journals.aps.org/prd/abstract/10.1103/PhysRevD.85.014034.

[80] B. B. Abelev, et al., Suppression of $\Upsilon(1S)$ at forward rapidity in Pb-Pb collisions at $\sqrt{s_{\rm NN}} = 2.76$ TeV, Phys. Lett. B 738 (2014) 361–372. arXiv:1405.4493, doi:10.1016/j.physletb.2014.10.001.

[81] V. Khachatryan, et al., Suppression of $\Upsilon(1S)$, $\Upsilon(2S)$ and $\Upsilon(3S)$ production in PbPb collisions at $\sqrt{s_{\mathrm{NN}}}$ = 2.76 TeV, Phys. Lett. B 770 (2017) 357–379. arXiv:1611.01510, doi:10.1016/j.physletb.2017.04.031.

[82] S. Acharya, et al., Υ production and nuclear modification at forward rapidity in Pb-Pb collisions at $\sqrt{s_{\mathrm{NN}}} = 5.02$ TeV, Phys. Lett. B 822 (2021) 136579. arXiv:2011.05758, doi:10.1016/j.physletb.2021.136579.

[83] P. Wang, Υ measurements in Au+Au collisions at $\sqrt{s_{NN}} =$ 200GeV with the STAR experiment, Nucl. Phys. A 982 (2019) 723–726. doi:10.1016/j.nuclphysa.2018.09.025.

[84] S. Voloshin, Y. Zhang, Flow study in relativistic nuclear collisions by Fourier expansion of Azimuthal particle distributions, Z. Phys. C 70 (1996) 665–672. arXiv:hep-ph/9407282, doi:10.1007/s002880050141.

[85] A. M. Sirunyan, et al., Measurement of the azimuthal anisotropy of Υ(1S) and Υ(1S) mesons in PbPb collisions at $\sqrt{s_{_{\mathrm{NN}}}} = 5.02$ TeV, Phys. Lett. B 819 (2021) 136385. arXiv:2006.07707, doi:10.1016/j.physletb.2021.136385.

[86] S. Acharya, et al., Measurement of Υ(1S) elliptic flow at forward rapidity in Pb-Pb collisions at $\sqrt{s_{\mathrm{NN}}} = 5.02$ TeV, Phys. Rev. Lett. 123 (19) (2019) 192301. arXiv:1907.03169, doi:10.1103/PhysRevLett.123.192301.

[87] A. Tumasyan, et al., Nuclear modification of Υ states in pPb collisions at $\sqrt{s_{\mathrm{NN}}}$ = 5.02 TeVarXiv:2202.11807.

[88] S. Chatrchyan, et al., Event Activity Dependence of Y(nS) Production in $\sqrt{s_{NN}}$=5.02 TeV pPb and $\sqrt{s}$=2.76 TeV pp Collisions, JHEP 04 (2014) 103. arXiv:1312.6300, doi:10.1007/JHEP04(2014)103.

[89] A. M. Sirunyan, et al., Investigation into the event-activity dependence of Υ(nS) relative production in proton-proton collisions at $\sqrt{s}$ = 7 TeV, JHEP 11 (2020) 001. arXiv:2007.04277, doi:10.1007/JHEP11(2020)001.

[90] S. Digal, P. Petreczky, H. Satz, Quarkonium feed-down and sequential suppression, Phys. Rev. D 64 (2001) 094015. arXiv:0106017.

[91] C. Lourenco, R. Vogt, H. K. Woehri, Energy dependence of J/psi absorption in proton-nucleus collisions, JHEP 02 (2009) 014. arXiv:0901.3054, doi:10.1088/1126-6708/2009/02/014.

[92] A. Abdulsalam, P. Shukla, Suppression of bottomonia states in finite size quark gluon plasma in PbPb collisions at Large Hadron Collider, Int. J. Mod. Phys. A 28 (2013) 1350105. arXiv:1210.7584, doi:10.1142/S0217751X13501054.

[93] T. Umeda, K. Nomura, H. Matsufuru, Charmonium at finite temperature in quenched lattice QCD , Eur. Phys. J. C 39S1 (2005) 9. arXiv:0211003.

[94] M. Asakawa, T. Hatsuda, J/ψ and η_C in the deconfined plasma from lattice QCD arXiv:0308034.

[95] S. Datta, F. Karsch, P. Petreczky, I. Wetzorke, Behavior of charmonium systems after deconfinement , Phys. Rev. D 69 (2004) 094507. arXiv:0312037.

[96] A. Jakovác, P. Petreczky, K. Petrov, A. Velytsky, Quarkonium correlators and spectral functions at zero and finite temperature, Phys. Rev. D 75 (2007) 014506. arXiv:0611017.

[97] C. Allton, M. B. Oktay, M. Peardon, J. Skullerud, Charmonium at high temperature in two-flavor QCD, Phys. Rev. D 76 (2007) 094513. arXiv:0705.2198.

[98] C. Y. Wong, Heavy quarkonia in quark gluon plasma, Phys. Rev. C 72 (2005) 034906.

[99] A. Mócsy, P. Petreczky, Quarkonia correlators above deconfinement, Phys. Rev. D 73 (2006) 074007. arXiv:0512156.

[100] A. Mócsy, P. Petreczky, Heavy quarkonia survival in potential model, Eur. Phys. J. C 43 (2005) 77. arXiv:0411262.

[101] W. M. Alberico, A. Beraudo, A. D. Pace, A. Molinari, , Phys. Rev. D. 76 (2007) 114506.

[102] D. Cabrera, R. Rapp, T-matrix approach to quarkonium correlation functions in the QGP, Phys. Rev. D 76 (2007) 114506. arXiv:0611134.

[103] A. Mócsy, P. Petreczky, Can quarkonia survive deconfinement ? , Phys. Rev. D 77 (2008) 014501. arXiv:0705.2559.

[104] A. Mócsy, P. Petreczky, Color Screening Melts Quarkonium, Phys. Rev. Lett. 99 (2007) 211602. arXiv:0705.2183.

[105] M. Laine, O. Philipsen, M. Tassler, Thermal imaginary part of a real-time static potential from classical lattice gauge theory simulations, JHEP 0709 (2007) 066. arXiv:0707.2458.

[106] M. Laine, A resummed perturbative estimate for the quarkonium spectral function in hot QCD , JHEP 0705 (2007) 028. arXiv:0704.1720.

[107] M. Laine, How to compute the thermal quarkonium spectral function from first principles?, Nucl. Phys. A 820 (2009) 25C. arXiv:0801.1112.

[108] N. Brambilla, J. Ghiglieri, A. Vairo, P. Petreczky, Static quark-antiquark pairs at finite temperature, Phys. Rev. D 78 (2008) 014017. arXiv:0804.0993.

[109] P. Petreczky, Recent progress in lattice QCD at finite temperaturearXiv:0906.0502.

[110] P. Petreczky, Quarkonium in Hot Medium, J. Phys. G. 37 (2010) 094009. arXiv:1001.5284.

[111] O. Kaczmarek, F. Karsch, P. Petreczky, F. Zantow, Heavy Quark Anti-Quark Free Energy and the Renormalized Polyakov Loop, Phys. Lett. B 543 (2002) 41. arXiv:0207002.

[112] M. Strickland, D. Bazow, Thermal Bottomonium Suppression at RHIC and LHC, Nucl. Phys. A 879 (2012) 25–58. arXiv:1112.2761, doi:10.1016/j.nuclphysa.2012.02.003.

[113] B. Krouppa, M. Strickland, Predictions for bottomonia suppression in 5.023 TeV Pb-Pb collisions, Universe 2 (3) (2016) 16. arXiv:1605.03561, doi:10.3390/universe2030016.

[114] B. Krouppa, A. Rothkopf, M. Strickland, Bottomonium suppression at RHIC and LHC, Nucl. Phys. A 982 (2019) 727–730. arXiv:1807.07452, doi:10.1016/j.nuclphysa.2018.09.034.

[115] A. Dumitru, Y. Guo, M. Strickland, , Phys. Lett. B 662 (2009) 37.

[116] O. Kaczmarek, F. Karsch, F. Zantow, P. Petreczky, , Phys. Rev. D 70 (2004) 074505.

[117] G. S. Bali, K. Schilling, A. Wachter, , Physical. Rev. D 56 (1997) 2566.

[118] R. L. Thews, M. Schroedter, J. Rafelski, Enhanced J/ψ production in deconfined quark matter, Phys. Rev. C 63 (2001) 054905. arXiv:hep-ph/0007323, doi:10.1103/PhysRevC.63.054905.

[119] G. Bhanot, M. E. Peskin, Short Distance Analysis for Heavy Quark Systems. 2. Applications, Nucl. Phys. B 156 (1979) 391–416. doi:10.1016/0550-3213(79)90200-1.

[120] F. Karsch, M. T. Mehr, H. Satz, Color Screening and Deconfinement for Bound States of Heavy Quarks, Z. Phys. C 37 (1988) 617. doi:10.1007/BF01549722.

[121] F. Arleo, P. B. Gossiaux, T. Gousset, J. Aichelin, Heavy quarkonium hadron cross-section in QCD at leading twist, Phys. Rev. D 65 (2002) 014005. arXiv:hep-ph/0102095, doi:10.1103/PhysRevD.65.014005.

[122] R. L. Thews, M. L. Mangano, Momentum spectra of charmonium produced in a quark-gluon plasma, Phys. Rev. C 73 (2006) 014904. arXiv:nucl-th/0505055, doi:10.1103/PhysRevC.73.014904.

[123] T. Affolder, et al., Production of $\Upsilon(1S)$ mesons from χ_b decays in $p\bar{p}$ collisions at $\sqrt{s} = 1.8$ TeV, Phys. Rev. Lett. 84 (2000) 2094–2099. arXiv:hep-ex/9910025, doi:10.1103/PhysRevLett.84.2094.

[124] R. Vogt, M. Prakash, P. Koch, T. H. Hansson, J/ψ Interactions With Hot Hadronic Matter, Phys. Lett. B 207 (1988) 263–268. doi:10.1016/0370-2693(88)90572-2.

[125] M. Gluck, E. Reya, A. Vogt, Pionic parton distributions, Z. Phys. C 53 (1992) 651–656. doi:10.1007/BF01559743.

[126] L. Grandchamp, S. Lumpkins, D. Sun, H. van Hees, R. Rapp, , Physical. Rev. C (2006) 0649006.

[127] R. Rapp, X. Du, Theoretical Perspective on Quarkonia from SPS via RHIC to LHC, Nucl. Phys. A 967 (2017) 216–224. arXiv:1704.07923, doi:10.1016/j.nuclphysa.2017.05.097.

[128] L. Grandchamp, R. Rapp, , Nucl. Phys. A 709 (2002) 415.

[129] C. Flores, , Talk at Quark matter 2017.